Development of Carbon Nanotube-Based Sensors—A Review

Benjamin Mahar, Cosmin Laslau, *Student Member, IEEE*, Ronnie Yip, and Yu Sun, *Member, IEEE*

***Abstract*—Carbon nanotubes (CNTs) have shown great promise as sensing elements in nanoelectromechanical sensors. In this review paper, we discuss the electrical, mechanical, and electromechanical properties of CNTs that are used in such applications. This investigation indicates which nanotube properties should be carefully considered when designing nanotube-based sensors. We then present the primary techniques that have been used for the integration of nanotubes into devices and proceed to give a description of sensors that have been developed using CNTs as active sensing elements.**

***Index Terms*—Carbon nanotubes (CNTs), integration, nanoelectromechanical systems (NEMS), sensors.**

I. Introduction

SINCE their discovery [1], carbon nanotubes (CNTs) have shown great promise for applications in the field of nanoelectromechanical systems (NEMS) that are devices integrating electrical and mechanical components with critical dimensions $\leq$ 100 nm. CNTs have been considered as possible replacements for silicon-based circuits due to their attractive electrical properties [2]. The fact that individual nanotubes can be either metallic conductors or semiconductors allows them to be used to construct transistors and the connections between transistors, which make up the components of integrated circuits. This can be a major boon as shrinking conventional CMOS silicon transistors is approaching fundamental physical limits. The potential implementation of these CNT-based circuits will allow for the continued reduction in transistor dimensions, an important factor for increasing IC performance.

Not only are the electrical properties of interest, CNTs also exhibit remarkable mechanical properties, possessing a tensile strength greater than any other known materials [3]. These unique properties have led to their use in areas as diverse as sensors, actuators, field-emitting flat panel displays, and energy and gas storage. The electrical, mechanical, and electromechanical properties of CNTs, and, in particular, how they can be applied towards constructing CNT-based NEMS sensors, are the focus of this paper.

In order for NEMS devices to be efficiently and reliably manufactured, the ability to accurately position CNTs on a substrate is of vital importance. Thus, it would be difficult to discuss CNT-based devices without considering the methods of integrating nanotubes into devices. Several methods have been developed for this purpose; generally, these methods can be divided under two broad subgroups: *in-situ* growth or postgrowth manipulation. *In-situ* growth techniques involve the use of catalytic particles patterned directly onto a substrate to control the positions in which CNTs are grown. Postgrowth manipulation techniques focus on moving previously synthesized nanotubes into their desired positions. Both methods are to be discussed, but the emphasis will be given to postgrowth techniques. With this understanding, the types of sensors that have been fabricated using CNTs will be subsequently described.

Manuscript received January 5, 2006; revised March 20, 2006. The Associate editor coordinating the review of this paper and approving it for publication was Dr. John Vig.

The authors are with the University of Toronto, Toronto, ON M5S 3G8, Canada (e-mail: sun@mie.utoronto.ca).

Color versions of one or more of the figures in this paper are available online at http://ieeexplore.ieee.org.

Digital Object Identifier 10.1109/JSEN.2006.886863

II. Carbon Nanotube Structure

The structure of the single-walled CNT can be considered as a single seamless, rolled up graphene sheet. The graphene sheet consists of a hexagonal lattice of carbon atoms. Single-walled nanotubes (SWNT) consist of a single such sheet with a typical diameter of 1–1.5 nm [4], while multiwalled nanotubes (MWNT) consist of many such sheets, with layers rolled up one inside the other, with typical diameters ranging from 5 nm to hundreds of nanometers [5]. The diameter of such tubes is strongly dependant on the size of the catalyst particles used to produce them [5].

If the structure is cut along its tube axis and unraveled into a planar sheet, the measure of the nanotube's chirality can be determined. This parameter, along with the tube diameter, has strong implications on the conductivity of the nanotube [6]. Imagine that, by cutting the nanotube structure along its tube axis, a graphene sheet is formed as shown in Fig. 1, where one side of the sheet coincides with the dashed tube axis on the left, and the other side of the sheet coincides with dashed tube axis on the right. The chiral vector $\mathbf{C}$ (Fig. 1) is obtained by connecting one carbon bonding site on the left tube axis to the coinciding carbon bonding site on the right tube axis, forming the circumference of the nanotube's circular cross section. That is, the origin (0,0) and point C correspond to the same point on the nanotube. This vector is specified by a pair of integers (n, m) that relate $\mathbf{C}$ to two unit vectors $\mathbf{a_1}$ and $\mathbf{a_2}$ ($\mathbf{C} = n\mathbf{a_1} + m\mathbf{a_2}$) [6]. If $n = m$, the nanotube is known as "armchair." The tube is called "zigzag" in the case where $m = 0$. For all other configurations where chiral angles ϕ (Fig. 1) are in between 0° and 30°, the tubes are of "chiral" type [6].

III. Electrical, Mechanical, and Electromechanical Characteristics of SWNT

A. Electrical Properties

It has been theoretically predicted that the properties of a nanotube are sensitively dependent on the tube diameter and chiral

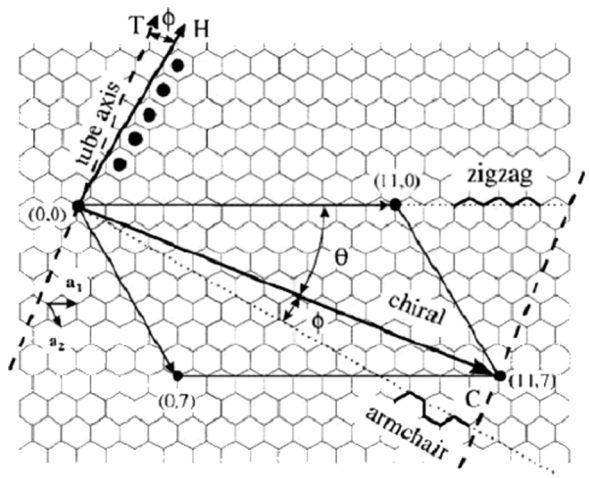

Fig. 1. Planar graphene sheet. Construction of the CNT can be achieved by rolling the sheet along the wrapping vector **C**, such that the origin coincides with point C, a nanotube indicated by indices (11,7) is formed [6].

angle, both of which are functions of n and m of the chiral vector **C**. Armchair nanotubes ($n = m$) are metallic. For all other tubes, there are two possibilities. If $n - m = 3N$ (where N is an integer), the tubes are expected to be metallic; otherwise, the tubes are semiconducting with an energy gap of approximately 0.5 eV [6]. In the semiconducting case, the energy gap is dependent on the tube diameter, with increasing diameters leading to decreased energy gaps [6].

Odom *et al.* [7] showed experimentally the metallic and semiconducting behaviors of different SWNTs. Fig. 2 shows selected results of the reported data. Using scanning tunneling microscopy (STM), they determined both the chiral angles and diameters of the different nanotubes, parameters that can easily be converted to n and m based on geometric considerations. Current versus voltage was then measured on specific sites along the nanotube. The near-constant, nonzero conductance (11,2) SWNT (Fig. 2, top) shows qualitatively that the nanotube is metallic, although the upturn in the I-V curve at higher biases shows that the metallic tubes retain a certain degree of semiconducting character. This upturn has been explained by the saturation of the current at high biases due to optical phonon scattering [8]. The behavior exhibited by a (14,3) SWNT (Fig. 2, bottom) shows that the nanotube is a moderate gap semiconductor. These results are in agreement with the predicted theoretical rules concerning the components of the chiral vector, illustrating the remarkable electronic property of a SWNT that subtle changes in its structure can alter the classification as either metallic or semiconducting.

Since the energy gap of the semiconducting SWNT is inversely proportional to its diameter, researchers are able to produce devices with different energy gaps, from 0 (metallic nanotubes) to more than 1 eV (which is roughly that of silicon) as well as values in between [2]. Thus, it is possible to control the bandgap energy without doping, which would be required in conventional silicon-based devices. Therefore, nanotube-based devices can be created that turn on and off at voltages customizable to a specific application.

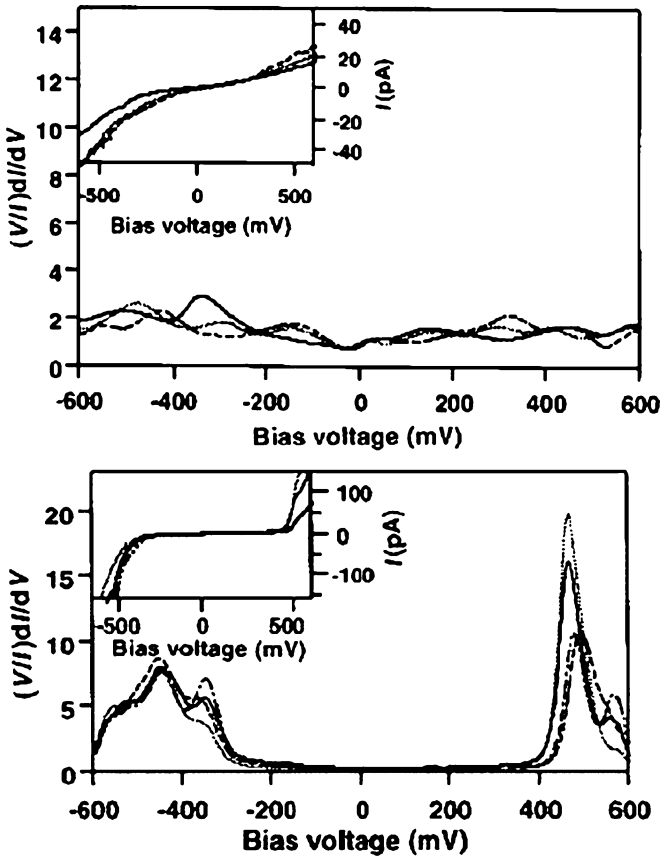

Fig. 2. Normalized conductance (V/I) dI/dV versus bias voltage V, and current I versus bias voltage V (inset). Top figure corresponds to a metallic (11,2) SWNT; the bottom, a semiconducting (14,3) SWNT. The various lines indicate the measurements obtained from different tube locations [7].

Due to their small diameters and large aspect ratio [2], CNTs are one-dimensional structures, exhibiting unique electronic characteristics. Resistance in most materials is largely due to conduction electrons colliding with defects in the crystal structure of the material. These collisions cause electrons to deviate from their paths. It is the scattering of these electrons that gives rise to resistance. Inside CNTs, electrons are not easily scattered. Since conduction electrons can only travel forwards or backwards, backscattering and scattering through defects are major causes of electrical resistance. For semiconducting nanotubes, backscattering is the major cause of resistivity, but for metallic nanotubes backscattering has been found to be largely absent. For high-quality metallic nanotubes, the major source of resistivity at low bias is scattering by acoustic phonons [9], which is a weak form of scattering. Thus, reduced scattering in metallic CNTs leads to their very low resistances [10].

High-quality metallic nanotubes at low biases ($<$200 meV) are ballistic conductors [11]. Low energy electrons can travel several micrometers without collision at room temperature although for higher biases the electrons are scattered by optical phonons, leading to a scattering distance that is more than 100 times shorter [12]. This is very striking when one considers that an excellent conductor such as copper has conduction electrons that will travel for about 40 nm, at most, before they scatter [2]. Semiconducting nanotubes can also achieve ballistic conduction on the scale of several hundred nanometers. Li *et al.*

have verified ballistic conductivity for several nanotubes measuring 0.4 cm in length [13], showing that the excellent low resistances of CNTs extend over large lengths. These results are consistent with a resistance of 6 kΩ/μm, which is applicable for lengths that can vary over four orders of magnitude. However, it should be noted that this resistance change is an approximation, as both experimental [14] and theoretical [15] studies have indicated that even over shorter scales of microns, the change in resistance with respect to length is nonlinear. The overall excellent conductivity is nevertheless important in exploiting nanotube properties over the various length scales over which a device may be designed to operate.

As has been shown by Collins *et al.*, electrical properties of SWNTs can undergo extreme changes in the presence of even small concentrations of gases such as oxygen [16]. Exposure to oxygen will change the resistance by a dramatic 10%–15%, presenting a number of implications. Among them is an application for chemical sensors, which will be discussed in Section VI-C. Perhaps more interestingly, this chemical sensitivity allows one to reversibly "tune" the resistance of an existing nanotube to a desired specification. For example, a hitherto semiconducting nanotube can be tuned into a metallic nanotube. Another implication is that the operating conditions of a device using nanotubes can have serious effects on its performance, a change that is potentially unwanted and that designers must take into consideration.

B. Mechanical Properties

Nanotubes possess remarkable mechanical properties because they are essentially rolled up graphene sheets. Graphite is exceptionally strong with respect to in-plane deformations and can support very large tension. Nanotubes have tensile strength that is unmatched by any other known materials [3]. Not only are nanotubes strong, but they are also extremely elastic. They can reversibly bend to very large angles [17].

Simulations of the mechanical properties of nanotubes have led to the conclusion that a 1 nm wide nanotube can be treated as a hollow cylinder, subjected to the laws of continuum mechanics [17]. This is true of bending, torsion, and compression. The atomic nature of the nanotube structure will only come into play for very large deformations or at the limit of extreme tension. Numerous experimental studies have also been made to determine the mechanical properties of nanotubes. In one such study, Salvetat *et al.* measured the elastic and shear moduli of SWNT ropes using atomic force microscopy (AFM) [3]. They used a suspended beam configuration to perform their measurements (Fig. 3). Using the AFM tip to apply a load on the SWNT ropes, which are essentially bundles of tubes packed together in an orderly manner, they obtained the deflection versus applied force data. Young's modulus and shear modulus were calculated based on these measurements. The results for several nanotube ropes, of varying diameters and suspended lengths, are presented in Table I. The mechanical properties of CNTs are largely independent of their chirality.

Mechanical properties differ significantly between SWNTs and MWNTs. Palaci *et al.* reported that the radial Young's modulus of MWNTs strongly decreases with increasing radius [18]. External radii of about 2 nm show a Young's modulus of about

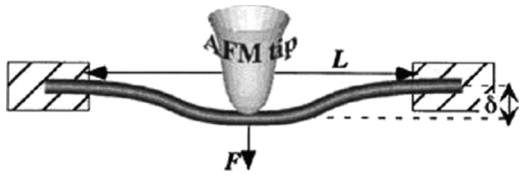

Fig. 3. Schematic of the Salvetat experiment: AFM is used to apply a load to the nanotube rope and to determine the resulting deflection [3].

TABLE I
DIAMETER D, SUSPENDED LENGTH L, SLOPE OF THE FORCE DEFLECTION CURVE, AND CALCULATED YOUNG'S AND SHEAR MODULI (Er AND G, RESPECTIVELY) OF THE NANOTUBE ROPES [3]

D (nm) ± 0.5nm	L (nm) ± 10%	$\Delta\delta/\Delta$F (m/N)	E_r (GPa) ± 50%	G (GPa) ± 50%
3.0	100	1.0	1310	…
3.0	140	4.0	899	…
4.5	285	9.3	642	…
4.5	180	3.0	503	6.5
6.0	200	1.8	369	2.9
6.0	230	3.0	332	1.7
9.0	180	0.5	189	2.3
13.5	360	0.5	298	2.8
13.5	360	1.0	149	0.9
20.0	370	0.5	67	0.7

400 ± 200 GPa, dropping off to an asymptotic value an order of magnitude lower at 30 ± 10 GPa for external radii 4 nm or greater. Considering mass production and repeatability, this shows the importance for sensors to use a homogeneous set of CNTs, both of type (SWNT versus MWNT) and of radius, as mechanical properties change dramatically as these variables are altered.

Because of their large tensile modulus (on the order of 1 TPa), nanotubes have often been discussed as potential target components of nanoscale fiber-reinforced composites for mechanical applications. They may either be dispersed individually, or be incorporated as filamentary bundles or ropes. One application is in composites, where carbon fiber type materials have been demonstrated as having the potential for unprecedented mechanical properties. Andrews *et al.* found that using a 5% loading of SWNTs, the resulting nanotube composite carbon fibers increased tensile strength by 90% and modulus by 150% [19].

The mechanical properties of nanotubes can be altered through controlled breakage. Marques *et al.* described the breakage of MWNTs through necking [20] in order to obtain an isolated SWNT; further tensile stress leads to the formation of a single chain of carbon atoms as the SWNT is in high tension, eventually leading to a total breakage. As opposed to the brittleness of graphite, they noted that some SWNTs exhibit an impressive elastic range, with an elongation of over 50%. This ductile behavior is attributed to vacancy defects within nanotubes. This change from brittle to ductile behavior shows yet again the flexibility of CNT properties, allowing for devices to use irradiated nanotubes [21] with special properties.

C. Electromechanical Properties

Due to the potential integration of CNTs in electromechanical devices (especially for sensors), the effect of mechanical defor-

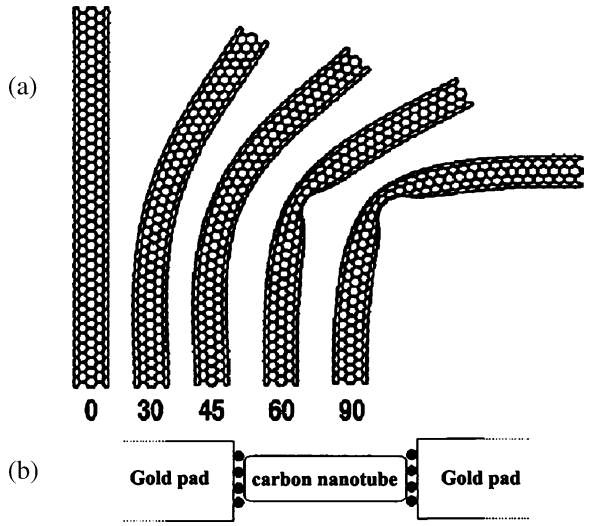

Fig. 4. (a) Structures of the isolated bent nanotubes used in the Rochefort calculations; numbers represent the bending angles (angle between the vertical and the bent segment). (b) Schematic of the model used in the computation [23].

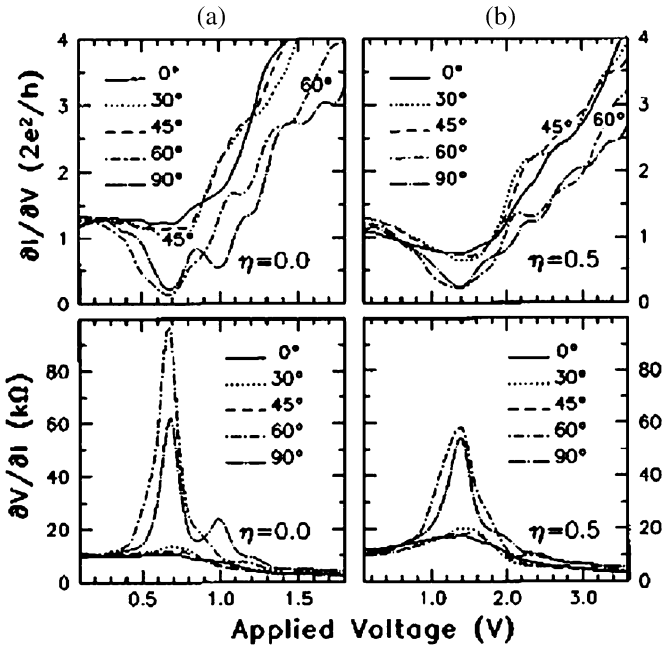

Fig. 5. Differential (top) conductance and (bottom) resistance of the bent tubes. (a) Case for $\eta = 0$ and (b) case for $\eta = 0.5$ [23].

mation on the electrical properties of CNTs has been of keen interest. Most of the research in this area has focused on metallic CNTs because it is mainly their changes in conductance, when a specific deformation is applied, that is of interest for NEMS sensor development.

A few early studies concluded that bending distortions of CNTs would have negligible effects on its electrical properties [22]. However, this was limited only to small distortions. Frequently, strong deformations and kinks are developed due to van der Waals forces between nanotubes and the substrate on which they are placed. The nanotubes tend to follow the curvature of the metal electrode on which they are placed and follow the topography of the substrate to maximize their adhesion energy [23]. Rochefort *et al.* [23] calculated the effects of large nanotube bending deformations on its electronic properties. A finite length armchair (6,6) CNT was modeled to be contained between two infinite gold pads [Fig. 4(b)]. A factor, η, was defined as the ratio of the average electrostatic potential of the nanotube and the applied voltage between the gold pads. When $\eta = 0$, it can be interpreted that one of the electrodes is weakly coupled to the nanotube, as when the nanotube is probed with an STM tip. For $\eta = 0.5$, the interpretation is that the electrode-nanotube-electrode coupling is strong and symmetric. Results of differential conductance and resistance versus the applied voltage for different bending angles are presented in Fig. 5.

From Fig. 5, it can be seen how the differential conductance curve changes as the bending angle of the nanotubes is varied; thus, the bending of nanotubes increases their resistance. For low bending angles, changes in conductance are small, which is in agreement with the earlier analytical studies of [22]. However, there exists a critical bending angle (between 45° and 60°) above which conduction in the nanotube decreases dramatically. At this critical bending angle, the strain is strong enough to lead to kinks. The conductance decrease is thought to be caused by $\sigma - \pi$ electron hybridization effects due to the increased curvature produced by high-angle bending [23].

Tombler *et al.* [24] conducted an experimental study on the effects of local-probe manipulations on the electrical properties of the nanotubes. This work is similar to the analytical study of Rochefort *et al.* [23], in the sense that nanotubes are being examined under bending conditions. The main difference, however, lies in the fact an AFM tip was used to cause the bending in the nanotube. The AFM tip not only caused global deformation in the nanotube structure, but also local deformation in the proximity of the tip. This local deformation was not considered in the Rochefort simulations, in which the structure was modeled to be uniformly bent.

The experimental setup in Tombler *et al.* [24] consisted of a metallic SWNT suspended over metal electrodes on a SiO_2/Si substrate. Part of the SWNT length was suspended over a trench etched into the SiO_2 surface. The mechanical bending of the suspended SWNT was achieved by the AFM tip located over the center of the nanotube, while its conductance was recorded at the electrodes (Fig. 6). The suspended nanotube was pushed into the trench as the device stage was moved upward; then it was retracted. This was repeated many times. The cyclic movement of the stage was accompanied by the measurement of the cantilever deflection ΔZ_c and the conductance of the nanotube sample as functions of time.

The cantilever deflection ΔZ_c, along with the initial tip-to-tube distance Z_0 and stage position Z, can be used to determine the nanotube deflection δ at the center point of the nanotube. This deflection, from simple geometry, is calculated as $\delta = (Z - Z_0) - \Delta Z_c$. The deflection δ, in turn, was used to define a global strain parameter $\sigma = [(4\delta^2 + l^2)^{1/2} - l]/l$, where l is the suspended nanotube length. This parameter is essentially the ratio of the change in length of the nanotube and its original length, assuming that the deflected SWNT is pivoted at the edges of the trench and forms a triangle with its original configuration. Another parameter, $\theta = \tan^{-1}(2\delta/l)$, is the angle

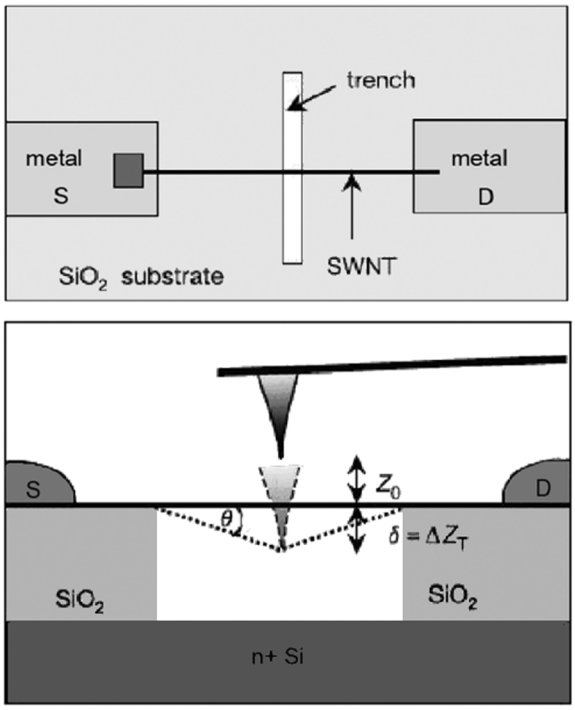

Fig. 6. Experimental setup of the Tombler experiment: (top) top view of the device and (bottom) side view of the AFM pushing experiment [24].

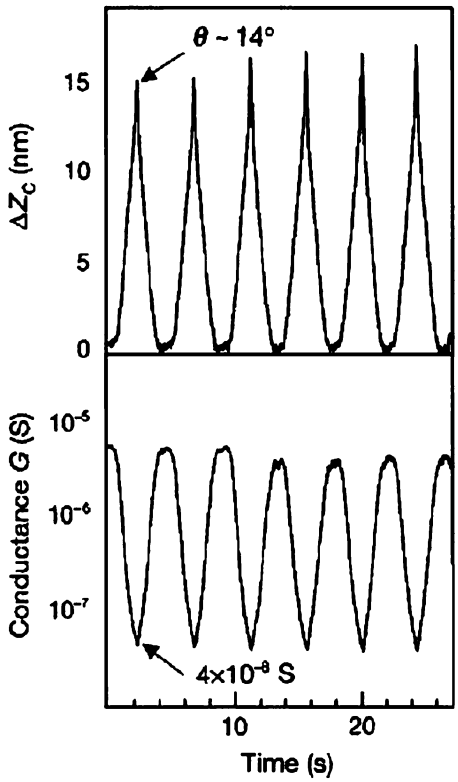

Fig. 7. Cantilever deflection and nanotube conductance during repeated cycles of pushing the suspended SWNT [24].

between the deflected nanotube and its undeflected configuration. Both of these parameters (σ and θ) were used to gauge the amount of deflection in the suspended nanotube beam.

The results shown in Fig. 7 describe the cantilever deflection ΔZ_c and conductance G as functions of time. The deflection shows a cyclic behavior as the stage was moved upward and retracted repeatedly. For this particular data set, the initial tip-to-tube distance Z_0 was 8 nm, and the stage moving range was 100 nm. The maximum beam and nanotube deflections were $\Delta Z_c \cong 15$ nm and $\delta \cong 76$ nm, respectively. It can clearly be observed from Fig. 7 that as the AFM tip pushes to deflect the nanotube, the tube conductance decreases continuously, and the conductance recovers as the tip is retracted. This is true during each cycle of the beam deflection. At the maximum nanotube deflection $\delta \cong 76$ nm, corresponding to $\sigma = 3\%$ and $\theta = 14°$, the conductance decreased by more than two orders of magnitude. This general behavior of increased bending leading to decreased conductance is in compliance with analytical predictions [24].

Similar studies were performed by Minot *et al.* [25]. Their results showed a comparable trend in conductance changes. Differences exist in the magnitude of conductance changes with strain and the minimum strain angle where a significant conductance change begin: for strain values of 2%, conductance decreased by about 35%. Recall that at 2% strain, Tombler *et al.* found a decrease of two orders of magnitude in conductivity. The variations can be attributed to the specific nanotube types used in the experiments.

It is interesting to note that both the electrical conductance and the mechanical deformations are highly reversible. The implication is that the observed change in sample conductance is due solely to the mechanical deformation of the nanotube caused by the tip movement [24]. This property implies that electromechanical nanotubes-based sensors can be made reliable over many use cycles.

Fig. 8 shows the conductance as a continuous function of global deformation strain σ, and deflection angle θ (inset). For small bending angles of $\theta \leq 5°$, conductance decreases slowly; then, at higher bending angles the decreases are much more significant. This data differs from the Rochefort simulations [23] that demonstrate a large drop in conductance will not occur unless the equivalent bending angle is at least about 22.5°.

The departure of the experimental results from the simulations is mainly due to the fact that the AFM tip causes the nanotube to change its atomic bonding configuration in the tip proximity. At small bending angles $(\theta \leq 5°)$, the SWNT retains sp^2 bonding throughout its entire structure [24]. As bending angle increases, larger structural changes occur directly underneath the AFM tip. In this case, the local bonding configuration near the tip will change from sp^2 to sp^3. Furthermore, the bending of the nanotube in the local region around the AFM tip causes a significant decrease in the number of π-electrons. Since these electrons are the main factor in electrical conductivity, we can conclude that the AFM tip's deflection effects (as opposed to a global change in CNT diameter) are responsible for the decrease in conductivity. No such tip effects were considered in the Rochefort simulations, where bending was considered to be uniform.

The conductance changed by two orders of magnitude at $\theta = 14°$ when using an AFM tip, which is contrasted by the predicted value that conductance changes only by tenfold at most,

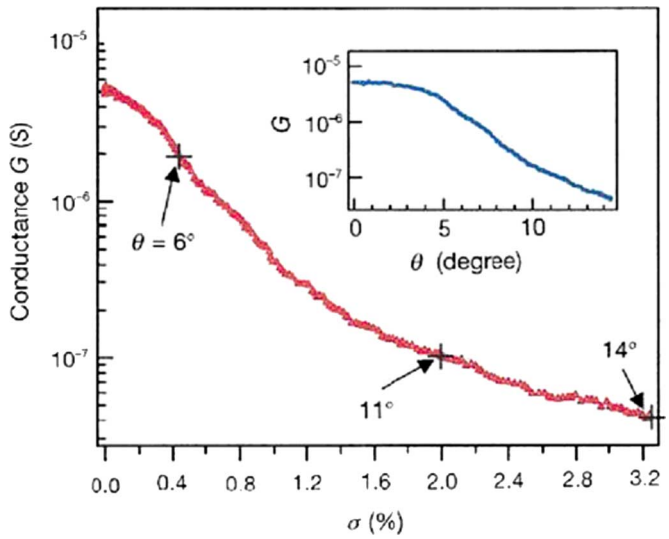

Fig. 8. Experimental results of SWNT conductance G versus strain σ. Inset shows its conductance G versus deflection angle θ. Note: σ does not scale linearly with θ [24].

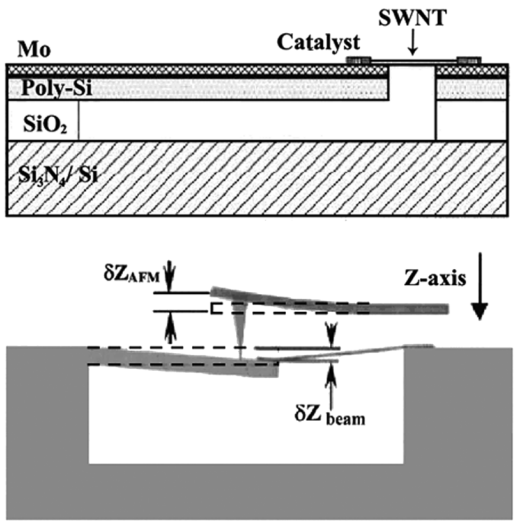

Fig. 9. (Top) Schematic of the device for nanotube stretching, catalyst on both sides of the suspended beam was used for nanotube growth. (Bottom) A tensile stretching mechanism utilizes an AFM tip applied on the cantilever [26].

at $\theta = 45°$, when using the Rochefort model where there is no tip involvement [24]. *The implication is that if one designs a sensor using bending nanotubes as the sensing mechanism, application of local probe (tip) manipulation should be considered in order to increase the sensitivity of the NEMS device.*

Cao *et al.* [26] investigated the electromechanical properties of SWNT under tensile stretching. Both metallic and semiconducting nanotubes were examined. They defined a nanotube as metallic only when $n = m$. If $n - m = 3N$, where N is an integer, they referred to the nanotube as *quasimetallic* (or small band-gap semiconducting, SGS-SWNT); otherwise, the nanotube is semiconducting. An experimental setup was devised to be similar to the one used in [24] for the local probe manipulation experiments. The setup consisted of an individual SWNT suspended over a micromechanical poly-silicon cantilever and a solid terrace. The SWNT rests on molybdenum (Mo) electrodes on both sides (Fig. 9). The silicon substrate can be applied with a voltage as it acts as a gate for the Mo source and drain.

To apply tensile stretching of the suspended nanotube, an AFM tip was used to push the cantilever, causing the cantilever to bend downwards. The tip was retracted once the desired beam deflection was obtained. This was repeated over numerous cycles. The device allowed for uniform tensile stretching because no tip was in contact with the nanotube during manipulation. The beam deflection and electrical conductance changes were measured and recorded as functions of time.

By taking into account the vertical coordinate Z, the initial tip-to-cantilever distance Z_0, and the AFM tip deflection $\delta \mathrm{Z}_{\mathrm{AFM}}$, the beam deflection $\delta \mathrm{Z}_{\mathrm{BEAM}}$ can be calculated by geometric considerations. A global strain parameter σ was then defined by taking into account the beam deflection $\delta \mathrm{Z}_{\mathrm{BEAM}}$, the original suspended nanotube length, and the slack in the nanotube. This parameter is essentially the ratio of the change in nanotube length to its original length.

Without considering the stretching of the nanotube for the moment, the SGS-SWNT will exhibit a varying conductance at different gate voltages when bias voltage is held at a constant level. However, the conductance never reaches zero. For a semiconducting nanotube (S-SWNT) under similar conditions, the $I - V_{\mathrm{GATE}}$ characteristics of the tube behave like a P-type field effect transistor, in which there is no conductance at the gate voltage of 0 V (i.e., the OFF position). For a metallic nanotube (M-SWNT), conductance is constant at different gate voltages. These characteristics of the three types of nanotubes were shown experimentally by Cao [26].

Fig. 10 shows the results for the SGS-SWNT over repeated stretching. In this case, the gate voltage was held at 0 V, and the bias voltage was held at 10 mV. In Fig. 10(a), it can be seen that as the AFM deflection increased above 40 nm, the current suddenly dropped. Generally, for small strain $(\sigma < 1\%)$, the conductance in suspended SWNT was found to be highly reversible upon repeated stretching and releasing, which is the case for this SGS-SWNT [Fig. 10(a)]. However, beyond 1% strain, irreversible changes to the device conductance occurred [26]. The conductance decreased by about one order of magnitude at the maximum strain point. An initial resistance of R_0 was measured to be 250 kΩ for one nanotube. Using the above strain analysis, a normalized resistance change $(\delta \mathrm{R}/\mathrm{R}_0)$ versus strain σ curve was obtained [Fig. 10(b)]. This curve shows that resistance increases linearly for small strain $(\sigma < 0.2\%)$, and more dramatically at higher strains. The behavior is highly repeatable over continuous pushing cycles. The inset of Fig. 10(b) shows the data for a different SGS-SWNT with an initial resistance of $\mathrm{R}_0 = 300$ kΩ, also exhibiting similar characteristics.

Cao *et al.* [26] also performed similar experiments on semiconducting nanotubes (S-SWNT) and found that the piezoresistive effect is much less prominent compared to SGS-SWNT. This effect is even further diminished in the case of metallic nanotubes (M-SWNT). Cao *et al.* qualitatively explained these electromechanical characteristics through theories of band-gap changes. However, the results do not agree well quantitatively. The resistance changes in both metallic and quasimetallic tubes are larger than what is expected from band-gap theories. Although this is not clearly understood, they attempted to explain

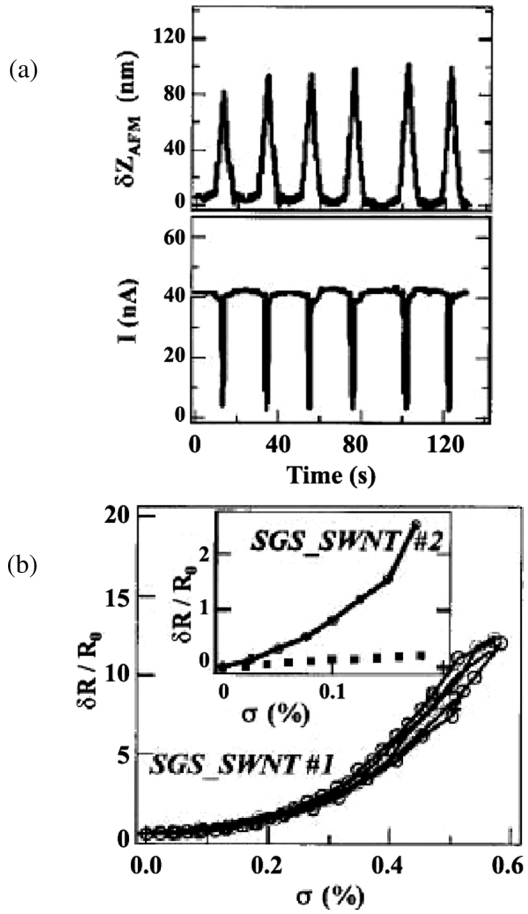

Fig. 10. (a) Experimental data of cantilever deflection and current for a SGS-SWNT. (b) Normalized resistance change versus strain for two different SGS-SWNTs [26].

the deviation by suggesting that there may be local deformations at the edges of the suspended beam. Also, contact resistance between the Mo electrodes and the nanotubes were relatively high, due to the slight oxidation of the electrodes.

These reported results demonstrate that *quasimetallic SWNTs are to be preferred for highly sensitive CNT-based strain sensors. The stretching mode of nanotube deformation is also to be preferred to the bending mode of deformation, as it displays greater resistance changes at lower strain while displaying a greater linearity in the changes.*

Conventional doped silicon strain gauges can have a piezoresistive gauge factor $(\delta \mathrm{R}/\mathrm{R}_0)/\sigma$ of approximately 200. This ratio can reach as much as 600 to 1000 in the linear range of quasimetallic SWNTs [26]. The gauge factor of CNTs has also been shown to be affected by doping. For example, films of CNTs doped with iodine changed their piezoresistive gauge factor from 65 in undoped films to 125 for doped films [27]. Individual SWNTs should be similarly affected, due to the effect that doping has on the Fermi level and density of states of SWNTs [28].

IV. CNT Growth and Electrode Contact Integration

Reliable synthesis techniques of CNTs are essential for the yielding of nondefective materials in desirable quantities. The challenge also lies in producing nanotubes with specific properties (n, m) for a specific application. Current synthesis techniques produce statistical distributions of chiralities, and, thus, electrical properties [7]. The difficulty in obtaining uniform electrical properties is a hurdle for the development of CNT-based electronics [29]. Early methods of nanotube production involved techniques such as electrical arc discharge and laser ablation to produce nanotubes of the highest quality in terms of graphitic structure [30]. The high processing temperature ensures perfect annealing of defects in the graphene sheets. This is especially important in the synthesis of multiwalled CNTs (MWNT) in which defects are more likely to occur. However, these methods also produce unwanted metal catalysts. Nanotubes must be selectively removed from the mixture. Other disadvantages of these techniques are that they are relatively slow and expensive and are, therefore, not suitable for mass production [30].

Structural defects in SWNTs are low irrespective of production methods [30]. Hence, alternative methods are often used for their synthesis. Chemical vapor deposition (CVD) is used as a method for SWNT growth at much lower temperatures compared to the two aforementioned techniques. CVD techniques are categorized according to their energy source type. The technique is called thermal CVD when a heat source such as a resistive or inductive heater is used. CVD without prefix commonly refers to thermal CVD. Plasma enhanced CVD (PECVD) is also used for nanotube growth where a plasma source is used to create a glow discharge. PECVD has the advantage of compatibility with semiconductor processing due to its even lower temperature requirements.

Metal catalysts are needed for nanotube growth by CVD or PECVD. Experiments showed that nanotube diameters have strong correlations with the catalyst particle size. Besides metal catalyst particles, metal film catalysts can be (and are) used, since at the high CNT growth temperatures, the films "ball up" into particle-like forms. For this technique, there is a critical film thickness beyond which no tubes will grow, a thickness which increases with substrate temperature [31]. Studies have shown metals that can be used as catalysts include Fe, Ni, Co, and Mo [30].

For SWNTs grown off patterned catalysts on flat silicon substrates, the locations from which the SWNTs emanate can be controlled by catalyst positioning. However, their orientations are random. Directed growth of SWNTs parallel to the plane of the substrate is first accomplished by Cassell et al [32]. Suspended SWNTs were grown from catalyst particles placed on top of regularly patterned silicon tower structures. A piece of polydimethylsilonxane (PDMS) elastomer was processed in an oxygen plasma, then it was spin coated with a liquid-based catalyst precursor [Fig. 11(a)]. The liquid precursor contains small amounts of iron and molybdenum chloride in its mixture. The elastomer, acting as an "inked" stamp, was pressed down onto a silicon substrate containing regular arrays of towers produced by photoresist patterning and anisotropic etching [Fig. 11(b)]. The transferred catalysts were dried in an oven at 60 °C for 5 min. The substrate was then heated in air at 400 °C for 4 h, followed by calcination to remove the polymer component which appeared in the liquid precursor [Fig. 11(d)]. The SWNTs were produced on the substrate by CVD using methane at 900

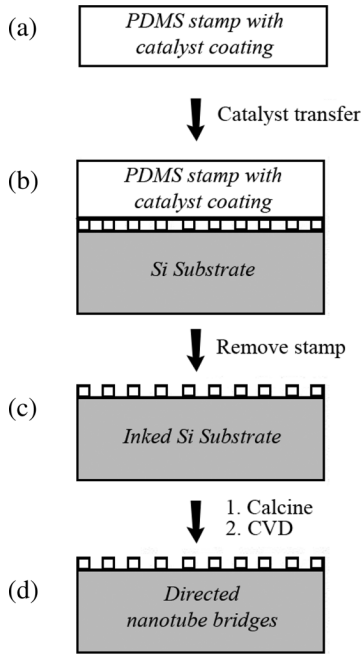

Fig. 11. Schematic procedures for directed growth of suspended SWNTs [32].

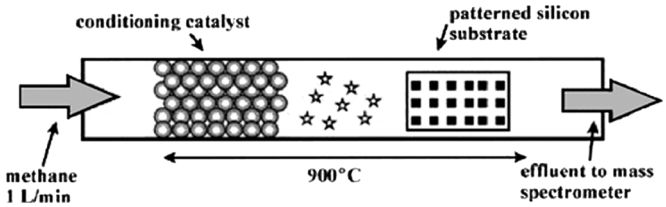

Fig. 12. Schematic experimental setup for enhanced CVD growth of SWNTs [33].

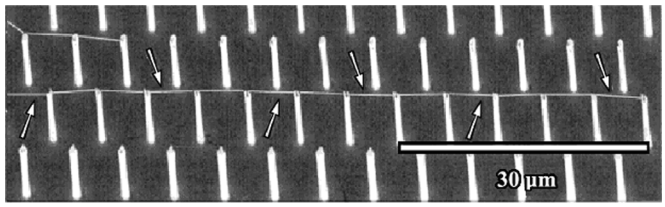

Fig. 13. In-plane growth of CNTs. The image shows a 100-μm-long nanotube grown along towers [33].

°C using a methane flow of 750 mL/min for 20 min [32]. This process resulted in highly directional suspended SWNTs. Their directions are determined by the pattern of the towers.

The yield of the directed growth method [32] is less than desirable. Interconnected nanotubes on the towers forming square patterns only existed in scattered regions of the substrate. Correspondingly, Franklin *et al.* [33] provided an "enhanced" CVD growth technique for high-yield growth of SWNTs. Extensive networks of suspended SWNTs with a high-degree of orientation were obtained. This process is very similar to the directed CVD approach [32]. In this enhanced technique, substrates used for nanotube growth were once again lithographically patterned so that the wafers contained elevated features (towers). The stamping process was used to coat the tower tops with a liquid catalyst precursor. After calcinations, CVD growth was carried out. The enhancement comes from a bulk amount of conditioning catalyst (consisting of high surface area γ-alumina loaded with iron oxide and molybdenum oxide) that was placed upstream of the catalytically patterned substrate during the CVD process (Fig. 12). The resulting yield is much higher than the original synthesis approach. Using the enhanced system with the upstream conditioning catalysts, a larger number of nanotubes were grown off the towers on the downstream substrate, leading to more extensive networks of interconnected tube-tower structures. With this enhanced technique, individual SWNTs with length of up to 0.15 mm can be synthesized [33]. These long SWNTs normally cross many towers in a straight line along the CVD flow direction, as shown in Fig. 13. It was explained that the conditioning process enhances SWNT growth by activation of methane.

In this process, SWNTs were nucleated only on the tower tops since the catalytic stamping methods do not place catalysts on the underlying substrate. As SWNTs lengthen, the methane flow keeps the nanotubes floating since the flow velocity near the bottom surface is much lower than that near the tower tops. Hence, the nanotubes cannot be "caught" by the bottom surface. The adjacent towers serve as "attachment points" for the growing nanotubes. If the waving nanotubes contact these attachments points, the van der Waals interaction between the nanotubes and towers will hold the floating tubes in place [33].

Research into vertically aligned CNTs has also been conducted, using both plasma enhanced CVD and thermal CVD. These out-of-plane nanotubes, shown in Fig. 14, have potential as field emitters in applications such as scanning probes, microwave amplifiers, and parallel electron-beam lithography [34]. Aside from the orientation, which can offer advantages for certain device designs, PECVD allows for a significant lowering of temperatures, ranging from room temperature to 100 °C [35]. Such flexibility may prove to be critical for certain nanotube-based sensor applications. The plasma sources for PECVD can vary, ranging from DC to RF to microwave to inductively coupled plasma reactors. As shown by Bower *et al.* [36], the electric field arising from plasma significantly straightens the growth of the CNTs. Using a microwave plasma of acetylene and ammonia, they grew vertically aligned CNTs. Upon turning this field off, the growth was no longer strictly vertical, becoming instead randomly oriented and coiled.

Thermal CVD has also been shown to produce vertically grown CNTs. Lee *et al.*, for example, placed metal domains on a silicon substrate. When the density of metal domains reached a certain value, steric hindrance caused the CNTs to initiate vertically aligned growth [37].

The central idea of nanotube integration is to create electrical contacts between a nanotube and the substrate, thereby creating nanotubes-based devices. Several methods for establishing such contacts after nanotube growth on a substrate have been demonstrated. Tombler *et al.* [24] used an approach involving methods derived from Soh *et al.* [38] and Kong *et al.* [39]. First, a trench was photolithographically patterned onto a silicon wafer oxidized with a layer of SiO_2. The substrate was then coated with polymethylmethacrylate (PMMA). Using electron-beam lithography, the PMMA layer was patterned to form wells at both sides

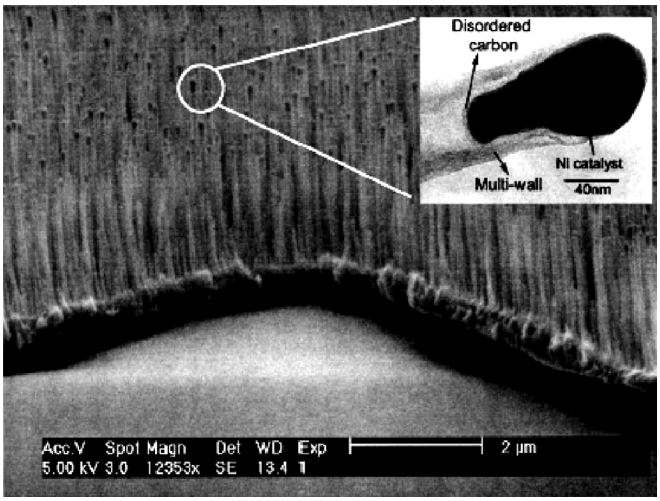

Fig. 14. Array of out-of-plane grown nanotubes [34].

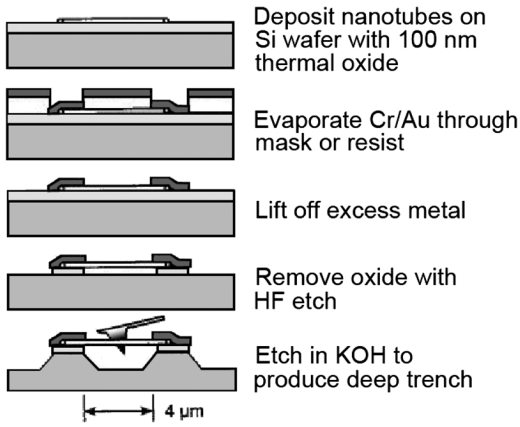

Fig. 15. Ropes of SWNTs pinned, then released by wet etching [40].

of the trench. After development, a few drops of suspended catalyst material were placed on the surface of the substrate, filling the exposed PMMA wells. After the solvent dried, the remaining PMMA was removed by liftoff, leaving patterned catalyst islands. This method for forming the catalyst pattern is different from the aforementioned catalyst "stamping" technique [32], [33] used for directed growth. Nanotubes were then grown by CVD from one catalyst island to the other. The final step was electron-beam lithography once again to place electrical contact pads (Ti 15 nm/Au 60 nm) over the catalyst islands. The contact pads fully covered the islands and extended over their edges by about 0.5 μm. It was found that contacts formed in this manner often have desired low resistance, ranging from 20 kΩ to several MΩ [38].

Another integration technique involves chemical etching of the substrate. Walters *et al.* [40] suspended a rope of SWNTs between electrode pads (Fig. 15). Ropes containing tens to hundreds of SWNTs bound by van der Waals forces were grown by laser vaporization. These ropes were suspended in a solvent. The Si substrate with a 100 nm thermally grown SiO_2 layer was dipped in the SWNT suspension to adhere the nanotube ropes to the substrate. The rope-covered surface was then masked using a copper grid. Chromium and gold were alternately evaporated through the mask to form electrode pads that pinned the ropes to the surface. Liftoff was performed to remove the copper mask. Regions of the oxide not covered by the electrodes were etched in HF to expose the silicon. Finally, a wet anisotropic etch in KOH removes a silicon thickness of 0.5–1.5 μm around the electrodes pads, leaving the rope of SWNTs to freely suspend over the trench. It is important to note that *the nanotubes were not seriously affected by the etching processes*.

Nygard and Cobden [41] used almost an identical approach to create electrical contacts of an individual SWNT (instead of ropes) suspended over a trench. CVD was used to grow nanotubes directly onto the substrate. Instead of using a copper mask for the evaporation of chromium and gold onto the nanotube ends, they instead opted for electron-beam lithography patterned PMMA. After liftoff of the PMMA, only one HF wet etch step was used to etch the SiO_2 layer, leaving the nanotube suspended. No anisotropic etch was performed afterward. The wet isotropic etch was terminated by transferring the substrate to water and then isopropanol, followed by drying in a nitrogen steam. The main difference here, compared to the Walters method [40], is that there is significant undercut underneath the raised electrodes due to the SiO_2 isotropic etching. Under certain circumstances, the nanotubes were suspended between the electrodes, while in other instances, they ended up draping across the bottom of the trench. Nygard and Cobden theorized that several factors influence the rate of successful suspension, including trench depth and width, firmness of the pinning to the electrodes, the straightness or the thickness of the tubes or bundles, and the drying procedures [41].

The methods involving wet etching are not suitable for long (> 0.5 μm) *suspended nanotubes*. Due to forces related to viscous fluidic flow or surface tension, wet etching tends to pull the suspended tubes. For long nanotubes, they often sag or are swept away after the wet processing steps [42].

Franklin *et al.* [42] developed an approach for the integration processing of suspended nanotubes that circumvents wet integration procedures. Molybdenum (Mo) is compatible with high-temperature SWNT growth. Therefore, if Mo electrode pairs were first fabricated onto the silicon substrate, SWNTs can be subsequently grown from electrodes to opposing electrodes to form bridges that are electrically connected to the Mo catalysts. The process starts with Mo film being deposited onto an oxidized substrate by sputtering, resulting in a 50 nm Mo film. Photolithography and dry etching form two opposing Mo electrodes. Photoresist was used as an etch mask for wet etching the exposed SiO_2 with a buffered HF solution. This step forms trenches around the Mo electrodes. The photoresist was subsequently removed so that catalysts can be patterned on top of the Mo electrodes. The patterning of catalysts involves electron-beam lithography. After the two catalyst islands were formed on top of the Mo electrodes, CVD of methane was used for the directed growth of the nanotube from one electrode to the other. The suspended nanotube synthesized in this manner is inherently electrically connected to the electrodes. The use of Mo was the key in this process as this material seems to be the *only* metal capable of withstanding the high CVD temperatures, while still being compatible with the CNT growth chemistry. Other metals

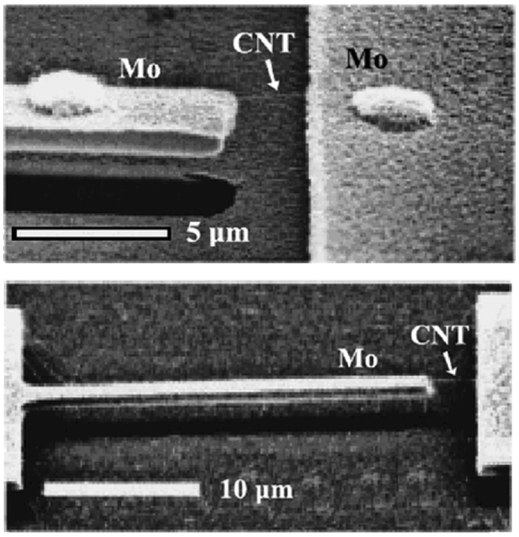

Fig. 16. CNT grown across a cantilever gap [42].

that have been attempted for use as pregrowth electrodes, such as gold, titanium, tantalum, and tungsten, have been less successful [42]. For example, titanium and tantalum partially etch during the CNT growth process, thereby increasing the electrodes' resistivity to unusable levels.

Franklin *et al.* found that the Mo electrodes exhibited excellent conductivity after growth and allowed for ohmic contacts with nanotubes. Measured resistivity was 20 kΩ to 1 MΩ, which matches the previously mentioned Ti/Au electrodes of Soh *et al.* [38]. Because no postgrowth processing is required, this technique is versatile in creating various structures. Fig. 16 shows an example of a nanotube suspended over a cantilever and a terrace.

Although resistance was low at the contact points following the nanotube growth, over time, this no longer seemed to be the case. The relative increase in resistance is thought to be due to the slight oxidation of the Mo in ambient conditions.

From a theoretical perspective, ballistic metallic nanotubes, when ohmically contacted, can at best display two units of quantum conductance; this leads to a resistivity limit of 6.5 kΩ [43]. By using palladium contacts for semiconducting single-walled CNTs, Dai *et al.* were able to reach unprecedented low levels of contact resistivity, with values consistently reaching 10 kΩ for 300-nm-long nanotubes of varying diameters [44]. The authors note that length is critical, as resistivity increased in longer nanotubes to 37 kΩ. They also theorize that acoustic phonons could account for the extra resistivity, and that low temperatures should allow for the resistivity to approach 6.5kΩ. This work was subsequently verified by Chen *et al.* who tested over one hundred single-walled CNT-based field effect transistors [45]. Of the three metals investigated as possible electrode materials (gold, titanium, and palladium), the authors conclude that Pd contacts provide the best performance.

As the aforementioned contact resistance research shows, significant work has been done to improve electrode-nanotube interaction, with palladium contacts being the most promising recent development. Nevertheless, various factors (e.g., type of metal, temperature, positioning, CNT length) can affect contact resistance, making contact resistance remain a serious concern for CNT-based sensor designers.

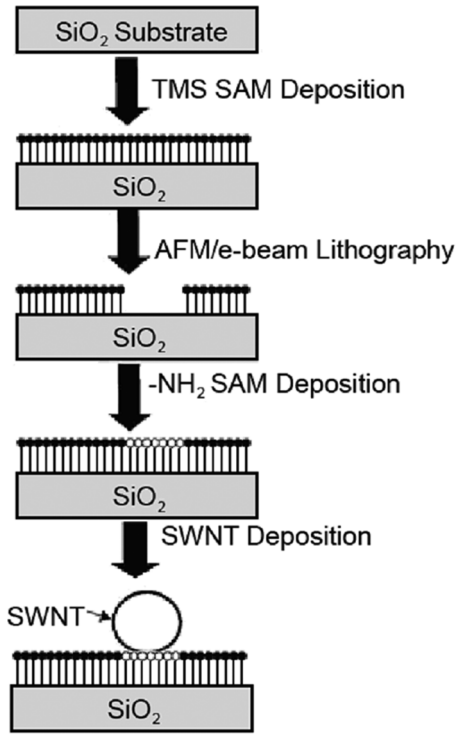

Fig. 17. Schematic diagram of controlled deposition of SWNT on chemically functionalized lithographic pattern [46].

V. Postgrowth Manipulation

A. Self-Assembly and Surface Functionalization

SWNTs can be grown from patterned catalysts deposited on top of raised structures (e.g., patterned SiO_2 towers). The growth method involves either thermal CVD or plasma enhanced CVD [30]. These methods seem to be capable of reasonably controlling the locations and orientations of the nanotube placements. However, if one works with a sample of already prepared SWNTs, the challenge remains in accurately and predictably *depositing* the nanotubes at the desired locations. Several methods have been explored for postgrowth manipulation.

Liu *et al.* [46] reported a method of depositing SWNTs on chemically functionalized nanolithographic templates. A suspension of nanotubes approximately 1 μm long was produced by sonicating purified SWNTs in N, N-dimethylformamide (DMF). The sequence of controlled SWNT deposition is shown in Fig. 17. An oxidized Si sample was functionalized with methyl-terminated $(-CH_3)$ self-assembled monolayer (SAM) by immersion in pure hexamethyldisilazane (HMDS) for 5 h at 150 °C. After this treatment, the sample surface is completely covered with a trimethylsilyl (TMS) monolayer. The sample was then patterned by electron-beam lithography to expose patterns on the TMS layer. A second SAM layer was prepared on the exposed SiO_2 pattern by functionalization with 3-aminopropyltriethoxysilane (APTES). This resulted in NH_2-terminated SAM layers filling in the electron-beam

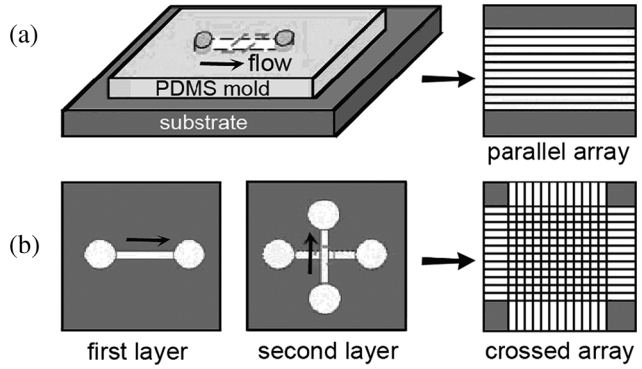

Fig. 18. Schematic of fluidic channels for flow assembly. (a) Nanowire assembly is carried out by flowing a suspension of NWs inside the channel. (b) Multiply crossed NWs can be obtained by changing flow direction sequentially [47].

exposed patterns (Fig. 17). The chemically patterned surface was soaked in the nanotube suspension for 10 min, and rinsed with methanol afterwards. SWNTs were preferentially attracted to the $(-NH_2)$ functionalized surfaces, while no SWNTs were observed on the $(-CH_3)$ functionalized surfaces [46]. Assembly of nanotubes on patterned substrates showed that the nanotubes often bridge or loop around patterned areas without precise directional control [47].

Lewenstein *et al.* [48] demonstrated that the surface functionalization technique is a useful method for positioning nanotubes in between pairs of electrodes, achieving near to 100% rate for the placement of a nanotube in the desired region, but only 20%–50% of the nanotubes formed electrical contacts with the electrodes due to the inability of shorter tubes to span their electrode gaps. It has also been demonstrated that this process can be used for the production of large numbers of nanotube-based circuits using a conventional microfabrication process [49]. The limiting factor for the circuits is the success rate with which electrical contacts can be assured. Greater purity nanotube suspensions and smaller electrode gaps would enable an increase in the success rate at which reliable electrical contacts are formed with this method.

B. Fluidic Manipulation

Huang *et al.* [47] investigated a technique of utilizing fluidic alignment to assemble silicon nanowires (NW) into parallel arrays on a substrate. For the purposes of this nanotube-oriented review, it should be noted that Huang *et al.* [47] suggested that nanotubes can be interchanged with nanowires with no loss of generality of the described techniques. Huang *et al.* developed nanowire arrays by passing suspensions of the nanowires (NWs suspended in ethanol solutions) through fluidic channel structures formed between a PDMS mold and a flat SiO_2/Si substrate [Fig. 18(a)]. The substrate used in flow assembly was functionalized with an NH_2-terminated SAM (both nanotube and nanowire attracting) layer by immersion in APTES for 30 min.

Parallel arrays of nanowires were achieved with a single flow. These arrays showed that the nanowires were all virtually aligned in the same direction as the flow. The nanowire alignments extended over hundreds of micrometers, and were limited by the length of the fluidic channels. The degree of alignment was controlled by fluidic flow rate. With increasing flow rates, the amount of nanowires deviating from the flow direction decreased. Additionally, the nanowire surface coverage within the channels can be controlled by flow durations. Huang *et al.* showed that the nanowire density increased with increasing flow durations [47].

Nanowires can be organized into complex crossed arrays with the use of a "layer-by-layer" scheme. For example, the formation of crossbar structures can be achieved by alternating the flow in orthogonal directions in a two-step assembly process. This required that the nanowire-substrate interaction is sufficiently strong that sequential flow steps do not affect the preceding ones [47]. Again, the spacing of the crossbars was controlled by flow durations, and the alignment by flow rates. Even more complex structures, such as an equilateral triangle of nanowires was obtained by a three step assembly process.

Similarly, Salalha *et al.* [50] studied nanowire alignment using a dilute drop of nanowire solution within a microchannel. However, the flow in this case was caused by thermocapillary motion. Thermocapillary motion operates on the principle of creating a temperature gradient, which, in turn, creates a difference in surface tension between the front and rear menisci of the droplet. As the droplet moved, most of the nanowires (85%) aligned themselves with the streamlines, and some were deposited on the substrate surface due to adhesive surface forces. If they were not, they were collected by the rear meniscus and orbited around for another cycle. By altering the direction of the gradient, there was flexibility in choosing the ultimate nanowire orientation. Although demonstrated only for nanowires, the technique will most probably be applicable to CNTs.

There are a number of factors [50] that must be controlled for the Salalha *et al.* technique to be effective. The rear contact line of the droplet causes changes in alignment and absorption of the nanowires, sometimes resulting in alignments quite different (45° off) than the direction of the thermocapillary motion. The study also found that due to the use of rectangular microchannel cross sections, a sink-source-like flow developed along the microchannel corners, causing a small percentage of nanowires to be concentrated in corners. Finally, the surface had to be appropriately patterned, which will vary depending on the type of devices to be constructed.

Overall, fluidic-assisted assembly has a number of control issues. Perhaps most importantly, even though alignment of nanowires with respect to the fluid flow direction is adequate, the separation between the individual nanowires is quite random (Fig. 19). *This makes us believe that if used, most applications involving fluidic alignment would require combination with another technique in order to achieve precise positioning control along both planar axes.*

C. Dielectrophoretic (DEP) Manipulation

Dielectrophoresis is the movement of neutral particles in a nonuniform electric field due to the frequency dependant polarization of these particles in the electric field [51]. Smith *et al.* [52] used a DEP assisted assembly technique to position individual nanowires onto the surface of a dielectric layer. As with other techniques initially demonstrated using nanowires, Smith

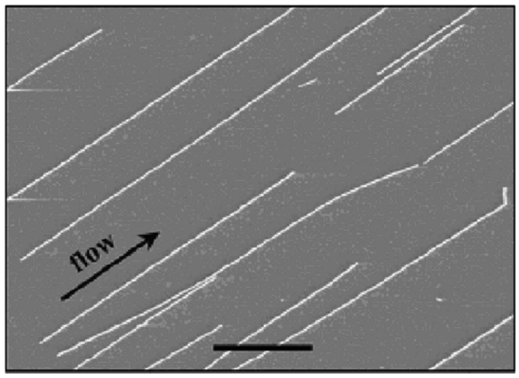

Fig. 19. Random distribution of nanowires aligned in the flow direction. The scale bar is 2 μm in length [50].

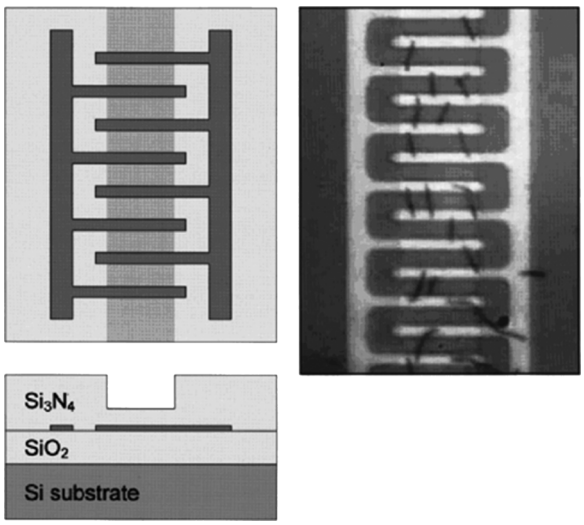

Fig. 20. (Left) Top and cross section views of the electrode structures used in field assisted assembly; (right) random distribution of vertically aligned nanowires across the electrode fingers [52].

et al. suggested that dielectrophoresis alignments can also be applied to *metallic* CNTs. Their strategy involved first depositing metal electrodes by liftoff onto a SiO_2 substrate (Fig. 20). These metal electrodes consisted of lithographically patterned interdigitated fingers made up of 50 nm Ti/150 nm Au. A layer of silicon nitride was then deposited by PECVD over the electrodes to prevent the formation of a short circuit by the nanowires during the assembly process. A narrow trench was etched immediately above the fingers to increase the field strength in this area above the electrodes (Fig. 20, left). As an alternating voltage ranging from 5 to 70 $V_{\rm rms}$ was applied to the electrodes, a suspension of nanowires was dispensed onto the silicon nitride layer. The resulting nanowire alignment is shown in Fig. 20 (right). The electrode to the left was applied with a voltage of 30 $V_{\rm rms}$ at a frequency of 1 kHz relative to the right grounded electrode; 200-nm diameter Au nanowires were used.

Alignment occurred in a direction perpendicular to interdigitated fingers over the thinned layer of silicon nitride. The length of time required for alignment decreased as the root mean square (rms) voltage was increased. The nanowires were distributed randomly along the electrode fingers. To achieve alignment at fixed locations, small square electrodes were deposited on top

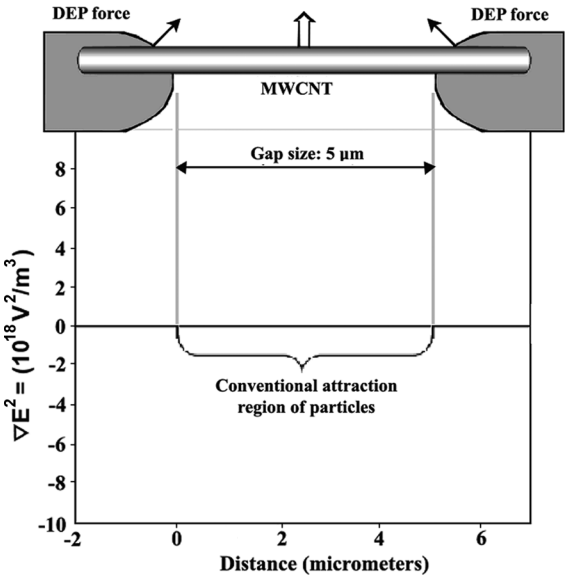

Fig. 21. Computationally resolved electric field gradient for a set of rounded electrodes showing the lack of dielectrophoretic force in the region of overlap between the electrodes and an MWCNT [55].

of the thinned silicon nitride layer at the center of the electrode fingers. Capacitive coupling between the lower and the upper electrodes resulted in an electric field strength that was higher near the top center electrodes than in the surrounding areas [52]. The resulting nanowires were aligned along the centers of the interdigitated fingers, bridging alternating pairs of adjacent electrodes. Voltages must be kept low ($< 25\ V_{\rm rms}$); otherwise, random alignment along the fingers as observed previously would occur.

Electrode size and geometry are two decisive factors in determining the precision with which nanotubes can be positioned. Sharper nanoelectrode tips provide a more sharply defined local maximum in the electric field and the nanotubes preferentially align in these regions [53]. Also, longer nanotubes move more easily than shorter nanotubes and impurity particles at higher frequencies in the electric field due to the increased length of the dipole moment [54], thus by controlling DEP frequency it can be assured that nanotubes and not impurity particulates will span the electrode gap.

Using DEP to trap nanotubes that are longer than the electrode gap, one would encounter problems due to the lack of dielectrophoretic force where the nanotube overlaps the electrodes (Fig. 21). Chung *et al.* [55] solved this problem by using a composite DC/AC field. Thus, the AC field attracted the nanotubes to their desired location while the DC field trapped them by electrostatic attraction. With a ratio of the DC field to the AC field of 0.348 at 5 MHz, they were able, with this technique, to achieve a single MWNT spanning the electrode gap with a 90% success rate.

A further refinement on the DEP positioning technique is the deposition of another layer of electrodes on top of the already DEP-trapped CNTs. Evoy *et al.* reported that after DEP-trapping CNTs using 100-nm-thick Ni/Cr bottom electrodes, a final lithography step is performed, to deposit 100-nm-thick top electrodes over the aligned nanotubes [56]. This additional

step serves two purposes. First, it improves the contact resistance between the CNT and the surrounding electrode assembly. Second, it "clamps" the nanotubes in place.

In addition to positioning, DEP has shown promise for the separation of nanotubes with different chiralities. Krupke *et al.* [57] have shown that semiconducting nanotubes can be separated from metallic nanotubes using DEP by exploiting the differences in their relative dielectric constants with respect to the solvent. The limiting factor in their separation process was that SWNTs dispersed in solvent tended to form bundles instead of individual tubes; thus, each bundle likely had both semiconducting and metallic tubes present.

The DEP process is promising due to precise manipulation of CNTs in a noncontact manner [58], although for this use it is vital to ensure the nanotubes are long enough to span the electrode gaps. For short nanotubes of a few hundred nanometers, an additional drawback is the requirement of extensive electron-beam lithography, which is a low-throughput process, to fabricate electrodes with a separation small enough such that the tubes can span the electrode gap [47].

D. Nanorobotic Manipulation

Nanorobotic manipulation involves the direct pick-and-place approach, individually directing CNTs for the creation of a device. Two main types of nanorobotic manipulation systems are based on atomic force microscopy (AFM) and scanning electron microscopy (SEM) or transmission electron microscopy (TEM).

AFM is one of the most important instruments serving as an interface between the macro and nano worlds, using a micro cantilever beam with a sharp tip to "feel" a sample surface. Deflections of the cantilever beam are typically detected by optical means. Using AFM as a sensor as well as a manipulator, nanomanipulation of nano objects were demonstrated [59]. However, AFM-based nanomanipulation is severely limited by an extremely low throughput and an inability of performing truly simultaneous imaging and manipulation. Performing nanomanipulation inside an SEM/TEM is a much more powerful technique, allowing for manipulating nanoscaled materials while providing simultaneous imaging capability.

Fukuda *et al.* [60] suggested that the main steps comprising this technique include preparation of nano building blocks, characterization of their properties, their placement with nanometer-scale resolution, and finally connecting the building blocks to form the final device. The enabling technologies for this technique are nanorobotic manipulators with multiple degrees of freedom, multiple independently actuated manipulators, and a real-time visual observation system. A nanorobotic system was constructed using piezoelectric-based nanomanipulators and a scanning electron microscope. The system operated with a sub-nanometer positioning resolution [60], demonstrating the ability to pick up an individual MWNT with an AFM cantilever tip and measure elasticity by buckling the tube. Furthermore, one end of a MWNT was positioned on the substrate, while the other end was on the cantilever tip. Moving the cantilever tip caused the MWNT to stretch and eventually rupture, leading to a method of destructive formation of sharpened MWNT tips.

Hone *et al.* [61] presented a nanorobotic process that aims towards the precise placement of a CNT with a specific set of characteristics. First, SWNTs were grown via CVD across a gap etched in a silicon wafer. The substrate was then used as a SWNT "cartridge" from which nanotubes can be taken. An AFM cantilever tip was used for manipulating the nanotubes, while simultaneously an SEM was used to image and guide the manipulation process. Once the nanotube was moved to the desired location using the AFM cantilever, the SEMs electron-beam was focused at the junction between the CNT and the substrate thus "welding" the nanotube into place.

Thus far, nanomanipulation is not suitable for large-scale manufacturing of NEMS devices; rather, it is extensively used in investigating fundamental properties and constructing proof-of-concept prototype devices [60]. For this type of research, nanorobotic manipulation provides flexibility. Using nanorobotic manipulation techniques, an individual CNT can be deformed through bending [62] or kinking [63], can be moved through sliding [64] or rolling [65], and can be broken [66]. Furthermore, by separating the high-temperature synthesis of CNTs from the creation of the nanodevice, substrates such as glass, plastics and CMOS chips can be used and compatibility can be maintained.

Looking towards large-scale manufacturing of NEMS devices, there are two main challenges for the nanorobotic manipulation approach. First, processes or control algorithms must be developed that are able to autonomously identify and work with CNTs of different sizes and properties, thereby selecting appropriate CNTs and positioning them without constant human intervention. Second, the low throughput of contemporary nanorobotic manipulation must be addressed, for example, through the adoption and control of dense arrays of end effectors for simultaneous, parallel manipulation [67].

VI. Carbon Nanotube-Based Sensors

We now present a survey of sensors that take advantage of the remarkable properties of CNTs. Typical of an emerging and rapidly developing field, there exist a multitude of proof-of-concept prototypes. However, less consideration has thus far been given to mass-production or field operation.

A. Temperature Sensors

Wood and Wagner [68] showed that CNTs embedded in polymer matrices exhibit a shift in the Raman D^* band with temperature. Fig. 22 shows the relationship between the peak position and the equilibrium temperature. It can be observed that the wavenumber of D^* band increases with decreasing temperatures as the nanotubes experience compression. Although these results demonstrate the possibility of using composite materials for temperature sensing, further work is required to improve the measurement repeatability. Specifically, the types of CNTs embedded within the polymer must be of a consistent type, in terms of chirality, diameter, length and number of walls. Furthermore, the dispersion and interconnectivity of the CNT network must also be relatively constant throughout the composite.

Relying on electrical properties rather than Raman shifts, Fung *et al.* [69] proposed a batch-fabrication technique for thermal sensors that used bundles of MWNTs as sensing elements. Using the DEP manipulation technique, they reported a

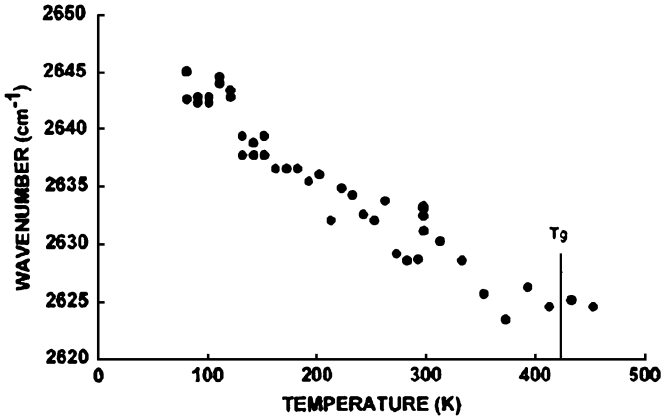

Fig. 22. SWNTs embedded in polycarbonate upon cooling [68].

70% success rate in placing the MWNT bundles onto fabricated Au electrodes. However, the results for the various individual sensors yielded resistance ranges from several kΩ to several hundred kΩ. *Similarly to the Wood and Wagner difficulties* [70], *this undesired variance was due to the unpredictability of using bundles of MWNTs and the inability to select whether metallic or semiconducting nanotubes were used.*

B. Flow Sensors

Ghosh *et al.* [71] presented a CNT-based flow sensor that is based on the generation of a current/voltage in a bundle of SWNTs when it was in contact with a flowing liquid. This induced current/voltage was earlier predicted by Kral and Shapiro in their theoretical investigation [72]. When the flow of free charged carrier induced in any material, an electric current is generated. In the case of CNTs, this generation is due to the transfer of momentum from the flowing liquid molecules so as to have a dragging effect on the free charge carriers in the nanotubes [71]. Although the predicted relationship between the electric current and the fluid flow velocity is linear, Ghosh *et al.* found experimentally that the induced voltage in fact fit logarithmic velocity dependence over nearly six decades of velocity [71]. The ionic conductivity and the polar nature of the liquid have great influence over the magnitude of the generated voltage. For flow velocities of the order of 10^{-5} m/s, saturation of the induced voltage was observed. The data collected was fitted empirically to a logarithmic equation. The experimental work by Ghosh *et al.* presented the great potential for CNTs as sensitive NEMS flow sensors.

C. Chemical Sensors

Kong *et al.* reported that at ambient temperatures, semiconducting SWNTs act as sensitive chemical sensors [73]. A single semiconducting SWNT was held in place by two electrodes. The electrodes were either Ti and/or Au. Using the two metal pads for electrical measurements, Kong *et al.* found that the conductivity of the semiconducting SWNT changed dramatically over several orders of magnitude when exposed to nitrogen oxide (NO_2) and ammonia (NH_3). Three orders of magnitude increase in conductivity was observed within 10 s after exposure of the SWNT to 200 ppm NO_2. The conductivity of the SWNT decreased by two orders within 2 min when the SWNT was exposed to a 1% NH_3 vapor [73].

It was explained that these responses were due to the charge transfer between the p-type semiconducting SWNT and the electron-donating NH_3 or electron-withdrawing NO_2 gas. Hole carriers were increased in the SWNT as it interacted with the NO_2 gas, causing an increase in conductance. The interaction with the NH_3 gas produced an opposite effect. Semiconducting SWNT gas sensor could be applied to other gases with electron donating or accepting capabilities. For example, as Collins *et al.* demonstrated, CNTs undergo dramatic electrical resistance changes in the presence of oxygen [16].

Many existing chemical sensors have the capability of sensing NO_2 and NH_3. However, these semiconducting metal oxide sensors must operate at high temperatures (up to 600°) for high sensitivity. In contrast, SWNT chemical sensors show strong responses even at room temperature, which is highly desired. However, the disadvantage with using a SWNT chemical sensor is that it needs to take several hours to release the analyte at room temperature before another sensing operation can be performed. This slow recovery remains a major drawback for nanotubes-based chemical sensors [73].

Li *et al.* addressed the concern of long recovery time with a sensor composed of SWNTs cast onto an interdigitated electrode [74]. The device, which had a detection limit of 44 ppb for NO_2 and 262 ppb for nitrotoluene, offers a detection response time on the order of seconds, similar to the sensor presented in [73]. The improvement is in recovery time, which was found to be on the order of minutes, by using ultraviolet light illumination to decrease the desorption-energy barrier. Sensing does not depend on the use of individual SWNTs, but rather a network or mesh of nanotubes, providing a large density and effective electrical contacts. Importantly, the variation in sensitivity between devices was found to be 6%, which demonstrates reproducibility superior to metal oxide or polymer-based sensors [75], [76].

The use of SWNT as chemical sensors has also been shown for other gases, with Chopra *et al.* demonstrating sensitivity to CO, N_2, He, O_2, and Ar, in addition to verifying the aforementioned NH_3 detection [77]. The device did not use changes in the electrical conductivity of the CNTs; rather, a circular disk resonator was constructed, which was coated with degassed nanotubes. These degassed nanotubes changed their dielectric constant when exposed to a gas. The authors reported a sensitivity of about 100 ppm and a response time smaller than contemporary sensors. The requirement for degassed nanotubes presents a limitation in terms of operating conditions, needing relatively high temperatures (125 °C) and low pressures (10^{-5} Torr). However, as other designs show [78], this is not an insurmountable problem. The detection of gases such as O_2 and CO_2 was demonstrated at room temperature conditions.

D. Biosensors

Techniques for molecular detection in biomedical applications must overcome the challenges of tissue penetration and the natural autofluorescent background of tissue and whole-blood media. To this end, near-infrared light between 0.9 and 1.3 eV has been used, for its greater penetration and for overcoming autofluorescence. Barone *et al.* used SWNTs for the creation

of such molecular detection sensors [79], taking advantage of the fact that CNTs fluoresce in the near infrared [80], a region in which human tissue and biological fluids are particularly transparent. A β-D-glucose-sensing model system was demonstrated, using an ultrasonicated and purified nanotube solution dialysed against surfactant-free buffer in the presence of glucose oxidase. This produces a porous layer of protein at the nanotube surface, which, in turn, interacts with the target analyte to moderate the fluorescence of the CNT. As the authors noted this approach has significant biomedical applications, including the construction of protein-nanotube sensors, DNA hybridization sensors, and active biomarkers.

Surface modification of nano-structures can be used for DNA detection, as demonstrated by Hahm and Lieber [81]. Using peptide nucleic acid receptors designed to recognize a specific mutation in a cystic fibrosis gene, the sensor was able to identify fully complementary versus mismatched DNA samples at extremely low concentrations. Although this very sensitive sensor was based on a silicon nanowire, the authors noted that given appropriate control over nanotube diameter and electrical properties, the same approach can be used for nanotube-based sensors. Dai and P. He chemically attached a single-strand DNA chain onto the surface of a CNT suspended on gold electrodes [82]. As in [81], this DNA-targeting surface modification allowed for the detection of complementary DNA and/or target DNA chains of specific sequences. Furthermore, thermally denaturing the complementary DNA from the nanotube surface allowed the sensor to be continuously reused. These studies point towards applications using nanotubes as sensing elements for biomedical analysis and diagnosis.

E. Pressure Sensors

Wood and Wagner [68] first demonstrated the potential of SWNTs as molecular and macroscopic pressure sensors. By using a diamond anvil cell, high hydrostatic pressures were applied to SWNTs. At the same time, the micro-Raman spectroscopy was recorded. The Raman spectra of specific materials show definite features that remain constant in air [i.e., certain peak intensities (bands) always occur at certain Raman wavenumbers]. In the case of the Wagner and Wood experiments [68], the Raman spectrum of the CNTs was monitored under different pressures to observe shifts in the various Raman bands. The use of macroscopic pressure in the diamond anvil cell allowed for the manipulation of the nanotube structures for comparison with the band shifts derived from the internal pressures of the fluid media. They found that the disorder-induced Raman peak of SWNTs (D^* band, 2610 cm^{-1} in air) shifted significantly as pressure was applied, relative to the corresponding peak in air (Fig. 23). There is some variance present in the measured wavenumbers, most probably due to the use of a bulk sample of CNTs, which contains nanotubes with large variations of properties such as chirality and diameter. Overall, since the observed shifts in Raman peaks are highly reversible, there is great potential for the use of CNTs in pressure sensing based on the mechanism of Raman band shifts, although the nanotubes' property-consistency issues still need to be resolved.

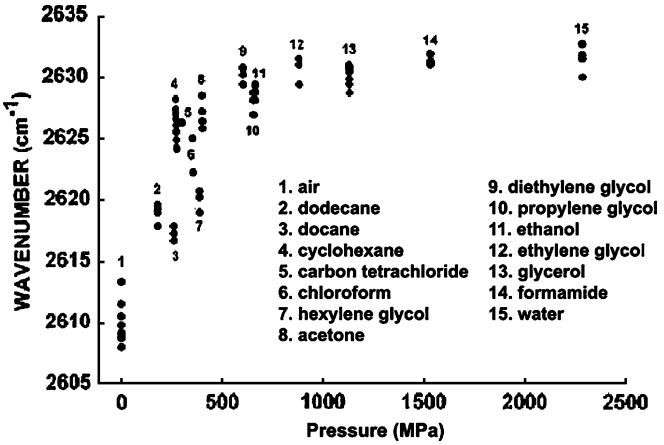

Fig. 23. Frequency shift of the D^* band in the Raman spectrum upon immersion of SWNT in various liquids [68].

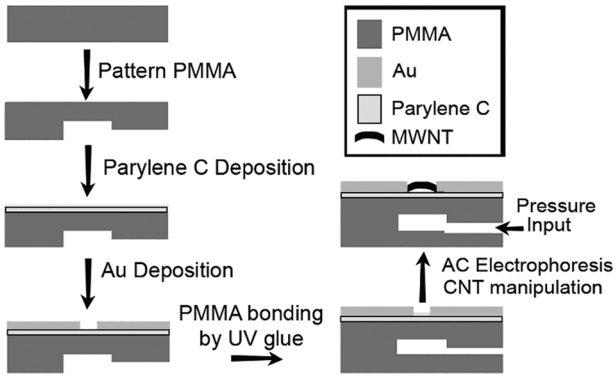

Fig. 24. Fabrication process flow for a CNT-based MEMS pressure sensor chip [83].

Fung *et al.* [83] developed a pressure sensor based on the piezoresitive properties of multiwalled CNTs. They used DEP to position a network of MWCNTs across a PMMA membrane, which was fabricated as indicated in Fig. 24. The deflection of the membrane under pressure caused a bending in the nanotubes. Gold electrodes were used with gap separations from 3 to 10 μm for DEP trapping. The advantage of this process is that since the entire device can be made through conventional micromachining processes, manufacturing the device can be done without resorting to low throughput electron-beam lithography. The disadvantage is that since the electrodes are relatively large, it is difficult to reproducibly obtain a single tube or a controlled number of tubes across the electrode gap. This, combined with the fact that the chiral properties of MWNTs are less well defined and that bundles of tubes instead of individual tubes were formed across the gap, would limit the reproducibility of the resistivity/pressure relationship across devices.

F. Mass Sensors

Volodin *et al.* [84] developed a mechanical resonant sensor using a coiled multiwalled CNT as a resonator. The structure for this device is a coiled MWCNT suspended between a pair of electrodes. The device was fabricated by locating a coiled

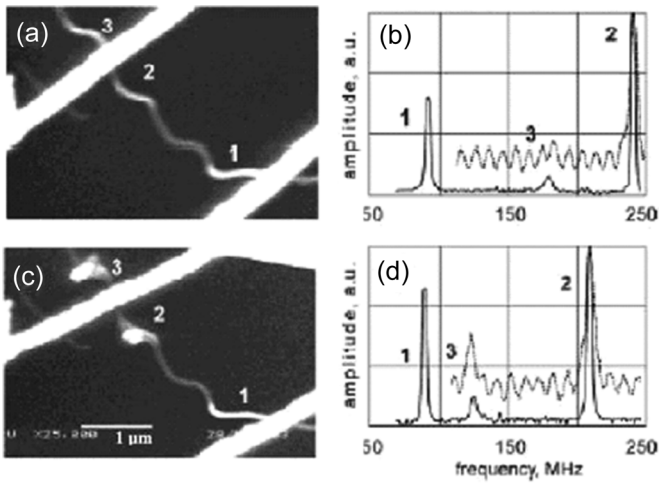

Fig. 25. SEM image shows (a) the coiled nanotube resonator originally, (c) and with added mass; (b), (d) the shift in the resonance frequency for the tw0 cases is shown to their right [84].

MWCNT on a substrate and then using electron-beam lithography and liftoff to define a pair of electrodes in contact with the coiled nanotube. Fig. 25 shows the device both unloaded [Fig. 25(a)] and with a carbon soot particle attached [Fig. 25(c)]. A radio-frequency (RF) circuit was connected to the electrodes to prove a measure of the generated signals and for generating excitations in the resonator. The frequency response of the resonator to an excitation caused by an AFM tip was obtained. Frequency response was also obtained for the same excitation after loading the resonator with carbon soot particles. It can be seen that the frequency response of the circuit after loading [Fig. 25(d)] shows the resonance peak shifts [Fig. 25(c)]. This demonstrates that such a device can prove useful for measuring masses in the range of 10 attograms; however, significant work would be required to obtain a reliable excitation method without using an AFM tip and external excitation sources. Additionally, the limited availability of coiled nanotubes would need to be addressed for such devices to gain practical usage.

Sazonova *et al.* reported self-detecting nanotube resonators [85], taking advantage of CNTs' ability to act as transistors. The device was constructed by growing a CNT between drain and source electrodes, suspended over a 500-nm-deep trench. Beneath this setup lies the gate, which uses an AC voltage to produce an oscillatory motion in the suspended nanotube. A resonance frequency of 55 MHz was measured, along with a quality factor of 80. Furthermore, by applying a DC offset via the gate, the nanotube was placed under tension, which, in turn, changed its oscillation frequency. The authors were thus able to tune the device, obtaining a resonant frequency that could be scaled from 3 to 200 MHz. The force sensitivity of the device is 1 fN/Hz$^{1/2}$, which is within an order of magnitude of the best force sensitivity ever measured at room temperature (0.1 fN/Hz$^{1/2}$ achieved by Jenkins *et al.* with magnetic-tipped silicon cantilevers [86]). The limiting factor is thermal vibration. Sazonova *et al.* predicted that at low temperatures of 1 K, forces below 5 aN could be detected, matching the highest sensitivities yet reported, which were achieved using ultrathin silicon cantilevers [87].

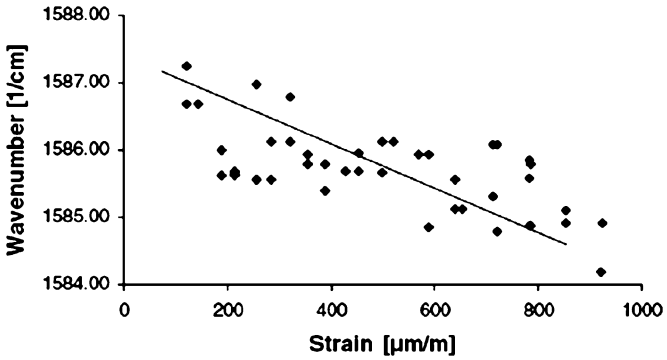

Fig. 26. G-band peak position for SWNTs in CNT film as a function of tensile strain (adapted from [89]).

G. Macroscopic Strain Sensors

The strong dependence of the SWNT's Raman band structure on mechanical deformations serves as the basis for the development of nanotube-based strain sensors. Zhao *et al.* [88] used CNTs embedded in a polymer to measure stress present in the polymer. They showed the potential of SWNT as strain sensors by relating the stress/strain of the nanotubes to the Raman band shift, although the complex setup makes it less practical for field operations. Li *et al.* [89] furthered this effort by using thin films of nanotubes as strain sensors. With the use of CNT films with isotropic properties applied to structural surfaces, macroscopic strain of the structure can be measured. In addition to using Raman spectroscopy to measure strain, they also showed that the voltage across the nanotube film varied with the strain on the film. The voltage/strain relationships are promising for practical applications because of the simpler setup involved. Such integration of CNT films into different materials not only results in sensors but can also achieve structural reinforcement.

In their experiments, Li *et al.* [89] attached a CNT film with randomly orientated bundles of SWNTs to a rubber strip using high-strength epoxy. The rubber strip was then loaded with tensile forces in order to induce axial strain in the nanotube film. A conventional strain gauge was applied to the other side of the specimen to measure the strain transferred to the film. Raman spectroscopy as well as four-point contact voltage measurements was performed on the film at different applied strain levels.

Fig. 26 shows results of the Raman wavenumber shift of the G band as a function of tensile strain. It can clearly be observed that an increase in tensile strain of the CNT films is accompanied by a decrease in the Raman wavenumber of the G band (i.e., a downward shift of the G band mode peak). Although the data is scattered, the general trend is clear. Fig. 27 shows results of the measured voltage-strain relationship. Li *et al.* concluded that strain in the nanotubes altered its electrical properties; therefore, CNT films can function as macroscopic strain sensors. The variability observed in both Figs. 26 and 27 arises from the nanotube film's disparity in properties such as constituent CNTs and CNT interconnectivity. Since four-point contact measurements in the experiments were performed at different locations of the film, differences in wavenumbers and voltages were obtained. As the authors noted, further work is necessary to re-

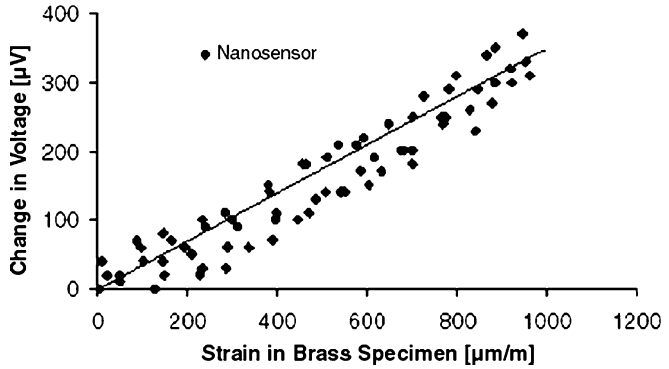

Fig. 27. Brass specimen, with a CNT film attached to it, subjected to tension: strain as a function of change in voltage in the CNT film [89].

duce this variability, by making the nanotube films more homogenous. Specifically, more consistency in nanotube properties (e.g., chirality and diameter) and a more uniform CNT network are necessary.

In addition to the aforementioned strain sensors based on CNT-embedded polymers or films, Raman spectroscopy can also be used to study strain in individual nanotubes. Cronin *et al.* used an AFM tip to create uniaxial strain in single-walled CNTs while monitoring the nanotubes with Raman spectroscopy [90]. The technique proved to be very sensitive, yielding detectable Raman shifts of 2 cm^{-1} for strains as low as 0.06%. Furthermore, the results showed that the Raman shifts due to strain are not consistent across all types of nanotubes. For nanotubes of metallic chirality, the radial breathing mode Raman spectra intensities vary significantly with strain. However, no such change was observed for semiconducting nanotubes.

VII. Conclusion

Our review/critique concludes that for CNT-based strain sensing applications the quasimetallic type nanotubes offer the greatest sensitivity. Furthermore, the stretching mode for CNTs is preferred over the bending mode due to its more sensitive and more predictable resistance changes in response to strain.

This paper has identified the two primary difficulties that must be dealt with in constructing a successful CNT-based sensor: CNT structure characterization and manipulation of the CNT structure. Although there is a wide-ranging toolset available to obtain the type of CNTs required, a method of producing a batch of nanotubes with identical electrical properties is still elusive. Thus, designers of CNT-based sensors must account for various distributions in the actual nanotube properties.

CNT post-growth manipulation methods were surveyed: self-assembly, fluidic flow, DEP, and nanorobotic manipulation. Of these, DEP was evaluated as achieving the best compromise between accurate placement and suitability for mass production. Uniquely, this advantage means that it can be implemented using conventional microfabrication technology. Perhaps most importantly, DEP also shows promise in the selectivity it exhibits towards the electrical properties of the deposited tubes.

Finally, this paper reviewed a range of nanotube-based sensors, focusing on mechanical pressure sensors and strain sensors. The vast majority of the surveyed devices were only in the prototype stage. Indeed, the process by which many of these devices were manufactured does not lend itself well to mass production. Thus, while prototypes have been showcased displaying remarkable advances, engineering research must be conducted before batches of reproducible, high-performance, cost-effective nanotube-based NEMS sensors can be produced and put into field operation, which is a current focus in the NEMS area.

References

[1] S. Iijima, "Helical microtubules of graphitic carbon," *Nature*, vol. 354, pp. 56–58, 1991.
[2] P. Avouris, "Supertubes," *IEEE Spectrum*, vol. 41, no. 8, pp. 40–45, Aug. 2004.
[3] J. P. Salvetat, G. A. D. Briggs, J. M. Bonard, R. R. Bacsa, and A. J. Kulik, "Elastic and shear moduli of single-walled carbon nanotube ropes," *Phys. Rev. Lett.*, vol. 82, pp. 944–947, 1999.
[4] A. Krishnan, E. Dujardin, T. W. Ebbesen, P. N. Yianilos, and M. M. J. Treacy, "Young's modulus of single-walled nanotubes," *Phys. Rev. B*, vol. 58, no. 20, pp. 14013–14019, 1998.
[5] M. P. Siegal, D. L. Overmyer, and P. P. Provencio, "Precise control of multiwall carbon nanotube diameters using thermal chemical vapor deposition," *Appl. Phys. Lett.*, vol. 80, pp. 2171–2173, 2002.
[6] J. W. G. Wildoer, L. C. Venema, A. G. Rinzler, R. E. Smalley, and C. Dekker, "Electronic structure of atomically resolved carbon nanotubes," *Nature*, vol. 391, pp. 59–62, 1998.
[7] T. W. Odom, J. L. Huang, P. Kim, and C. M. Lieber, "Atomic structure and electronic properties of single-walled carbon nanotubes," *Nature*, vol. 391, pp. 62–64, 1998.
[8] Z. Yao, C. L. Kane, and C. Dekker, "High-field electrical transport in single-wall carbon nanotubes," *Phys. Rev. Lett.*, vol. 84, pp. 2941–2944, 2000.
[9] C. L. Kane, E. J. Mele, R. S. Lee, J. E. Fischer, P. Petit, H. Dai, A. Thess, R. E. Smalley, A. R. M. Verschueren, S. J. Tans, and C. Dekker, "Temperature-dependent resistivity of single-wall carbon nanotubes," *Europhys. Lett.*, vol. 41, pp. 683–688, 1998.
[10] T. Ando, H. Matsumura, and T. Nakanishi, "Theory of ballistic transport in carbon nanotubes," *Phys. B*, vol. 323, pp. 44–50, 2002.
[11] A. Bachtold, M. S. Fuhrer, S. Plyasunov, M. Forero, E. H. Anderson, A. Zettl, and P. L. McEuen, "Scanned probe microscopy of electronic transport in carbon nanotubes," *Phys. Rev. Lett.*, vol. 84, pp. 6082–6085, 2000.
[12] J.-Y. Park, S. Rosenblatt, Y. Yaish, V. Sazonova, H. Ütüel, S. Braig, T. A. Arias, P. W. Brouwer, and P. L. McEuen, "Electron-phonon scattering in metallic single-walled carbon nanotubes," *Nano Lett.*, vol. 4, pp. 517–520, 2004.
[13] S. Li, Z. Yu, C. Rutherglen, and P. J. Burke, "Electrical properties of 0.4 cm long single-walled carbon nanotubes," *Nano Lett.*, vol. 4, pp. 2003–2007, 2004.
[14] P. J. de Pablo, C. Gómez-Navarro, J. Colchero, P. A. Serena, J. Gómez-Herrero, and A. M. Baró, "Nonlinear resistance versus length in single-walled carbon nanotubes," *Phys. Rev. Lett.*, vol. 88, no. 036804, 2002.
[15] A. N. Andriotis, M. Menon, and L. Chernozatonskii, "Nonlinear resistance dependence on length in single-wall carbon nanotubes," *Nano Lett.*, vol. 3, pp. 131–134, 2003.
[16] P. G. Collins, K. Bradley, M. Ishigami, and A. Zettl, "Extreme oxygen sensitivity of electronic properties of carbon nanotubes," *Science*, vol. 287, pp. 1801–1804, 2000.
[17] J. Bernholc, D. Brenner, M. Buongiorno Nardelli, V. Meunier, and C. Roland, "Mechanical and electrical properties of nanotubes," *Annu. Rev. Mater. Res.*, vol. 32, pp. 347–375, 2002.
[18] I. Palaci, S. Fedrigo, H. Brune, C. Klinke, M. Chen, and E. Riedol, "Radial elasticity of multiwalled carbon nanotubes," *Phys. Rev. Lett.*, vol. 94, no. 175502, 2005.
[19] R. Andrews, D. Jacques, A. M. Rao, T. Rantell, F. Derbyshire, Y. Chen, J. Chen, and R. C. Haddon, "Nanotube composite carbon fibers," *Appl. Phys. Lett.*, vol. 75, no. 9, 1999.
[20] M. A. L. Marques, H. E. Troiani, M. Miki-Yoshida, M. Jose-Yacaman, and A. Rubio, "On the breaking of carbon nanotubes under tension," *Nano Lett.*, vol. 4, pp. 811–815, 2004.
[21] F. Banhart, "Irradiation effects in carbon nanostructures," *Rep. Progr. Phys.*, vol. 62, no. 1181, 1999.

[22] C. L. Kane and E. J. Mele, "Size, shape, and low energy electronic structure of carbon nanotubes," *Phys. Rev. Lett.*, vol. 78, pp. 1932–1935, 1999.
[23] A. Rochefort, P. Avouris, F. Lesage, and D. Salahub, "Electrical and mechanical properties of distorted carbon nanotubes," *Phys. Rev. B.*, vol. 60, pp. 13824–13830, 1999.
[24] T. W. Tombler, C. Zhou, L. Alexseyev, J. Kong, H. Dai, and L. Liu, "Reversible electromechanical characteristics of carbon nanotubes under local-manipulation," *Nature*, vol. 405, pp. 769–772, 2000.
[25] E. D. Minot, Y. Yaish, V. Sazonova, J.-Y. Park, M. Brink, and P. L. McEuen, "Tuning carbon nanotube band gaps with strain," *Phys. Rev. Lett.*, vol. 90, p. 156401, 2000.
[26] J. Cao, Q. Wang, and H. Dai, "Electromechanical properties of metallic, quasimetallic, and semiconducting carbon nanotubes under stretching," *Phys. Rev. Lett.*, vol. 90, pp. 157601-1–157601-4, 2003.
[27] W. Wan-Lu, L. Ke-Jun, L. Yong, and W. Yong-Tian, "Piezoresistive effect of doped carbon nanotube/cellulose films," *Chin. Phys. Lett.*, vol. 20, pp. 1544–1547, 2003.
[28] E. Jouguelet, C. Mathis, and P. Petit, "Controlling the electronic properties of single-wall carbon nanotubes by chemical doping," *Chem. Phys. Lett.*, vol. 318, pp. 561–564, 2000.
[29] R. H. Baughman, A. A. Zakhidov, and W. A. de Heer, "Carbon nanotubes—the route toward applications," *Science*, vol. 297, pp. 787–792, 2002.
[30] M. Meyyappan, *Carbon Nanotubes: Science and Applications*. New York: CRC, 2005.
[31] Y. Y. Wei, G. Eres, V. I. Merkulov, and D. H. Lowndes, "Effect of catalyst film thickness on carbon nanotube growth by selective area chemical vapor deposition," *Appl. Phys. Lett.*, vol. 78, no. 10, pp. 1394–1396.
[32] A. M. Cassell, N. R. Franklin, T. W. Tombler, E. M. Chan, J. Han, and H. Dai, "Directed growth of free-standing single-walled carbon nanotubes," *J. Amer. Chem. Soc.*, vol. 121, pp. 7975–7976, 1999.
[33] N. Franklin and H. Dai, "An enhanced CVD approach to extensive nanotube networks with directionality," *Adv. Mater.*, vol. 12, pp. 890–894, 2000.
[34] W. H. Teh and C. G. Smith, "Integrating vertically aligned carbon nanotubes on micromechanical structures," *J. Vac. Sci. Technol. B.*, vol. 21, no. 4, pp. 1380–1383, 2003.
[35] M. Meyyappan, L. Delzeit, A. Cassell, and D. Hash, "Carbon nanotube growth by PECVD: A review," *Plasma Sources Sci. Technol.*, vol. 12, pp. 205–216, 2003.
[36] C. Bower, W. Zhu, S. Jin, and O. Zhou, "Plasma-induced alignment of carbon nanotubes," *Appl. Phys. Lett.*, vol. 77, pp. 830–832, 2000.
[37] C. J. Lee *et al.*, "Synthesis of aligned carbon nanotubes using thermal chemical vapor deposition," *Chem. Phys. Lett.*, vol. 312, pp. 461–468, 1999.
[38] H. T. Soh and C. F. Qate, "Integrated nanotube circuits: controlled growth and ohmic contacting of single-walled carbon nanotubes," *Appl. Phys. Lett.*, vol. 75, no. 5, pp. 627–629, 1999.
[39] J. Kong, H. T. Soh, A. M. Cassell, C. F. Quate, and H. Dai, "Synthesis of individual single-walled carbon nanotubes on patterned silicon wafers," *Nature*, vol. 395, pp. 878–881, 1998.
[40] D. A. Walters, L. M. Ericson, M. J. Casavant, J. Liu, D. T. Colbert, and K. A. Smith, "Elastic strain of freely suspended single-wall carbon nanotube ropes," *Appl. Phys. Lett.*, vol. 74, no. 25, pp. 3803–3805, 1999.
[41] J. Nygard and D. H. Cobden, "Quantum dots in suspended single-wall carbon nanotubes," *Appl. Phys. Lett.*, vol. 79, no. 25, pp. 4216–4218, 2001.
[42] N. R. Franklin, Q. Wang, T. W. Tombler, A. Javey, M. Shim, and H. Dai, "Integration of suspended carbon nanotube arrays into electronic devices and electromechanical systems," *Appl. Phys. Lett.*, vol. 81, no. 5, pp. 913–915, 2002.
[43] C. T. White and T. N. Todorov, "Carbon nanotubes as long ballistic conductors," *Nature*, vol. 393, pp. 240–242, 1998.
[44] A. Javey, J. Guo, Q. Wang, M. Lundstrom, and H. Dai, "Ballistic carbon nanotube field-effect transistors," *Nature*, vol. 424, pp. 654–657, 2003.
[45] Z. Chen, J. Appenzeller, J. Knoch, Y.-M. Lin, and P. Avouris, "The role of metal-nanotube contact in the performance of carbon nanotube field-effect transistors," *Nano Lett.*, vol. 5, pp. 1497–1502, 2005.
[46] J. Liu, M. J. Casavant, M. Cox, D. A. Walters, P. Boul, and W. Liu, "Controlled deposition of individual single-walled carbon nanotubes on chemically functionalized templates," *Chem. Phys. Lett.*, vol. 303, pp. 125–129, 1999.
[47] Y. Huang, X. Duan, Q. Wei, and C. Lieber, "Directed assembly of onedimensional nanostructures into functional networks," *Science*, vol. 291, pp. 630–633, 2001.
[48] J. C. Lewenstein, T. P. Burgin, A. Ribayrol, L. A. Nagahara, and R. K. Tsui, "High-yield selective placement of carbon nanotubes on prepatterned electrodes," *Nano Lett.*, vol. 2, pp. 443–446, 2002.
[49] S. G. Rao, L. Huang, W. Setyawan, and S. Hong, "Large-scale assembly of carbon nanotubes," *Nature*, vol. 425, p. 36, 2000.
[50] W. Salalha and E. Zussman, "Investigation of fluidic assembly of nanowires using a droplet inside microchannels," *Phys. Fluids*, vol. 17, pp. 063301-1–063301-5, 2005.
[51] H. A. Pohl, *Dielectrophoresis: The Behavior of Neutral Matter in Nonuniform Electric Fields*. Cambridge, U.K.: Cambridge Univ. Press, 1978.
[52] P. A. Smith, C. D. Nordquist, T. N. Jackson, and T. S. Mayer, "Electric-field assisted assembly and alignment of metallic nanowires," *Appl. Phys. Lett.*, vol. 77, no. 9, pp. 1399–1401, 2000.
[53] B. J. Nelson, L. Dong, A. Subramanian, B. Vikramaditya, and D. Bell, "Micro and nano assembly using dielectrophoretic forces," presented at the 3rd Int. Conf. Microchannels and Minichannels, Toronto, ON, Canada, Jun. 13–15, 2005, ICMM2005-75245, unpublished.
[54] K. Yamamoto, S. Akita, and Y. Nakayama, "Orientation and purification of carbon nanotubes using AC electrophoresis," *J. Phys. D: Appl. Phys.*, vol. 31, pp. 3403–3409, 1998.
[55] J. Chung, K.-H. Lee, J. Lee, and R. S. Ruoff, "Toward large-scale integration of carbon nanotubes," *Langmuir*, vol. 20, no. 8, pp. 3011–3017, 2004.
[56] S. Evoy *et al.*, "Dielectrophoretic assembly and integration of nanowire devices with functional CMOS operating circuitry," *Microelectron. Eng.*, vol. 75, pp. 31–42, 2004.
[57] R. Krupke, F. Hennrich, H. v. Löneysen, and M. M. Kappes, "Separation of metallic from semiconducting single-walled carbon nanotubes," *Science*, vol. 301, pp. 344–347, 2003.
[58] S. Evoy, N. DiLello, V. Deshpande, A. Narayanan, H. Liu, M. Riegelman, B. R. Martin, B. Hailer, J.-C. Bradley, W. Weiss, T. S. Mayer, Y. Gogotsi, H. H. Bau, T. E. Mallouk, and S. Raman, "Dielectrophoretic assembly and integration of nanowire devices with functional CMOS operating circuitry," *Microelectron. Eng.*, vol. 75, pp. 31–42, 2004.
[59] P. A. Williams, A. M. Patel, S. J. Papadakis, A. Seeger, R. M. Taylor, II, A. Helser, M. Sinclair, M. R. Falvo, S. Washburn, and R. Superfine, "Controlled placement of an individual carbon nanotube onto a MEMS structure," *Appl. Phys. Lett.*, vol. 80, no. 14, pp. 2574–2576, 2002.
[60] T. Fukuda, F. Arai, and L. Dong, "Assembly of nanodevices with carbon nanotubes through nanorobotic manipulations," *Proc. IEEE*, vol. 91, no. 11, pp. 1803–1818, Nov. 2003.
[61] J. Hone, X. M. H. Huang, R. Caldwell, L. Huang, S. C. Jun, M. Huang, M. Y. Sfeir, and S. P. O'Brien, "Controlled placement of individual carbon nanotubes," *Nano Lett.*, vol. 5, pp. 1515–1518, 2005.
[62] E. W. Wong, P. E. Sheehan, and C. M. Lieber, "Nanobeam mechanics: Elasticity, strength, and toughness of nanorods and nanotubes," *Science*, vol. 277, pp. 1971–1975, 1997.
[63] H. W. C. Postma, A. Sellmeijer, and C. Dekker, "Manipulation and imaging of individual single-walled carbon nanotubes with an atomic force microscope," *Adv. Mater.*, vol. 12, pp. 1299–1302, 2000.
[64] M. R. Falvo, R. M. Taylor, II, A. Helser, V. Chi, F. P. Brooks, S. Washburn, Jr., and R. Superfine, "Nanometer-scale rolling and sliding of carbon nanotubes," *Nature*, vol. 397, pp. 236–238, 1999.
[65] M. R. Falvo, J. Steele, R. M. Taylor, II, and R. Superfine, "Gearlike rolling motion mediated by commensurate contact: carbon nanotubes on HOPG," *Phys. Rev. B*, vol. 62, pp. R10665–R10667, 2000.
[66] M.-F. Yu, O. Lourie, M. J. Dyer, K. Moloni, T. F. Kelley, and R. S. Ruoff, "Strength and breaking mechanism of multiwalled carbon nanotubes under tensile load," *Science*, vol. 287, pp. 637–640, 2000.
[67] P. Vettiger, M. Despont, U. Drechsler, U. Dürig, W. Häerle, M. I. Lutwyche, H. E. Rothuizen, R. Stutz, R. Widmer, and G. K. Binnig, "The 'Millipede'—more than one thousand tips for future AFM data storage," *IBM J. Res. Develop.*, vol. 44, 2000.
[68] J. R. Wood and H. D. Wagner, "Single-wall carbon nanotubes as molecular pressure sensors," *Appl. Phys. Lett.*, vol. 76, no. 30, pp. 2883–2885, 2000.
[69] C. K. M. Fung, V. T. S. Wong, and W. J. Li, "Towards batch fabrication of bundled carbon nanotube thermal sensors," presented at the IEEE Nano Conf., 2003.
[70] J. R. Wood and H. D. Wagner, "Single-wall carbon nanotubes as molecular pressure sensors," *Appl. Phys. Lett.*, vol. 76, no. 30, pp. 2883–2885, 2000.
[71] S. Ghosh, A. K. Sood, and N. Kumar, "Carbon nanotube flow sensors," *Science*, vol. 299, pp. 1042–1044, 2003.

[72] P. Kral and M. Shapiro, "Nanotube electron drag in flowing liquids," *Phys. Rev. Lett.*, vol. 86, pp. 131–134, 2001.
[73] J. Kong, M. G. Chapline, and H. Dai, "Functionalized carbon nanotubes for molecular hydrogen sensors," *Adv. Mater.*, vol. 13, no. 18, pp. 1384–1386, 2001.
[74] J. Li, Y. Lu, Q. Ye, M. Cinke, J. Han, and M. Meyyappan, "Carbon nanotube sensors for gas and organic vapor detection," *Nano Lett.*, vol. 3, pp. 929–933, 2003.
[75] B. Matthews, J. Li, S. Sunshine, L. Lerner, and J. W. Judy, "Effects of electrode configuration on polymer carbon-black composite chemical vapor sensor performance," *IEEE Sensors J.*, vol. 2, no. 3, pp. 160–168, Jun. 2002.
[76] T. K. H. Starke and G. S. V. Coles, "High sensitivity ozone sensors for environmental monitoring produced using laser ablated nanocrystalline metal oxides," *IEEE Sensors J.*, vol. 2, no. 1, pp. 14–19, Feb. 2002.
[77] S. Chopra, K. McGuire, N. Gothard, A. M. Rao, and A. Pham, "Selective gas detection using a carbon nanotube sensor," *Appl. Phys. Lett.*, vol. 83, pp. 2280–2282, 2003.
[78] K. G. Ong, K. Zeng, and C. A. Grimes, "A wireless, passive carbon nanotube-based gas sensor," *IEEE Sensors J.*, vol. 2, no. 2, pp. 82–88, Apr. 2002.
[79] P. W. Barone, S. Baik, D. A. Heller, and M. S. Strano, "Near-infrared optical sensors based on single-walled carbon nanotubes," *Nature Mater.*, vol. 4, pp. 86–92, 2005.
[80] M. J. O'Connell *et al.*, "Band gap fluorescence from individual single-walled carbon nanotubes," *Science*, vol. 297, pp. 593–596, 2002.
[81] J. Hahm and C. M. Lieber, "Direct ultrasensitive electrical detection of DNA and DNA sequence variations using nanowire nanosensors," *Nano Lett.*, vol. 4, pp. 51–54, 2004.
[82] P. He and L. Dai, "Aligned carbon nanotube-DNA electrochemical sensors," *Chem. Commun.*, vol. 3, pp. 348–349, 2004.
[83] C. K. M. Fung, M. Q. H. Zhang, R. H. M. Chan, and W. J. Li, "A PMMA-based micro pressure sensor chip using carbon nanotubes as sensing elements," in *Proc. 18th IEEE Conf. Micro Electro Mechanical Systems*, 2005, pp. 251–254.
[84] A. Volodin, D. Buntinx, M. Ahlskog, A. Fonseca, J. B. Nagy, and C. Van Haesendonck, "Coiled carbon nanotubes as self-sensing mechanical resonators," *Nano Lett.*, vol. 4, no. 9, 2004.
[85] V. Sazonova, Y. Yaish, H. Ustunel, D. Roundy, T. A. Arias, and P. L. McEuen, "A tunable carbon nanotube electromechanical oscillator," *Nature*, vol. 431, pp. 284–287, 2004.
[86] N. E. Jenkins, L. P. DeFlores, J. Allen, T. N. Ng, S. R. Garner, S. Kuehn, J. M. Dawlaty, and J. A. Marohn, "Batch fabrication and characterization of ultrasensitive cantilevers with submicron magnetic tips," *J. Vac. Sci. Technol. B*, vol. 22, pp. 909–915, 2004.
[87] T. D. Stowe, K. Yasumura, T. W. Kenny, D. Botkin, K. Wago, and D. Rugar, "Attonewton force detection using ultrathin silicon cantilevers," *Appl. Phys. Lett.*, vol. 71, pp. 288–290, 1997.
[88] Q. Zhao, J. R. Wood, and H. D. Wagner, "Stress fields around defects and fibers in a polymer using carbon nanotubes as sensors," *Appl. Phys. Lett.*, vol. 78, no. 12, 2001.
[89] Z. Li, P. Dharap, S. Nagarajaiah, E. V. Barrera, and J. D. Kim, "Carbon nanotube film sensors," *Adv. Mater.*, vol. 16, no. 7, pp. 640–643, 2004.
[90] S. B. Cronin, A. K. Swan, M. S. Unlu, B. B. Goldberg, M. S. Dresselhaus, and M. Tinkham, "Resonant Raman spectroscopy of individual metallic and semiconducting single-wall carbon nanotubes under uniaxial strain," *Phys. Rev. B*, vol. 72, no. 035425, 2005.

Benjamin Mahar is currently in the Nanoengineering Program (Engineering Science) at the University of Toronto, Toronto, ON, Canada.

His current research is in the development of nanotube-based NEMS sensors. His research interests are in the areas of MEMS, nanofabrication, molecular biology, and nanomaterials.

Cosmin Laslau (S'05) is currently in the Nanoengineering Program (Engineering Science) at the University of Toronto, Toronto, ON, Canada.

His research stints consist of work on nanotube-based sensors at the University of Toronto, and work on quantum-dot lasers at the University of Wurzburg. His research interests also include the characterization of nanomaterials and the use of nanostructures in composite materials.

Ronnie Yip received the B.Eng. and M.Eng. degrees in mechanical engineering from McGill University, Montréal, QC, Canada in 2001 and 2003, respectively. He is currently pursuing the Ph.D. degree in mechanical engineering at the University of Toronto, Toronto, ON, Canada.

His research focuses on non-Newtonian fluid mechanics and rheology of elastic fluid flow past porous media.

Yu Sun (S'01–M'03) received the B.S. degree in electrical engineering from the Dalian University of Technology, China, in 1996, the M.S. degree from the Institute of Automation, Chinese Academy of Sciences, Beijing, China, in 1999, and the M.S. degree in electrical engineering and the Ph.D. degree in mechanical engineering from the University of Minnesota, Minneapolis, in 2001 and 2003, respectively.

He is Assistant Professor in the Mechanical and Industrial Engineering Department and is jointly appointed in the Institute of Biomaterials and Biomedical Engineering and Electrical and Computer Engineering Department, University of Toronto, Toronto, ON, Canada, where he established and directs the Advanced Micro and Nanosystems Laboratory. He held a Research Scientist position at the Swiss Federal Institute of Technology (ETH-Zürich) before joining the faculty of the University of Toronto. His research areas are MEMS design, fabrication and testing, microrobotic manipulation of biomaterials, cell biomechanics, nanofabrication, and nanorobotic manipulation of nanomaterials.

Dr. Sun is a recipient of the Ontario Early Researcher Award and the University of Minnesota Dissertation Fellowship.